

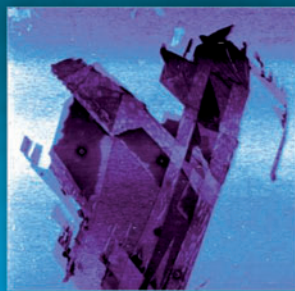
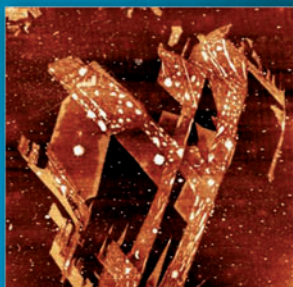
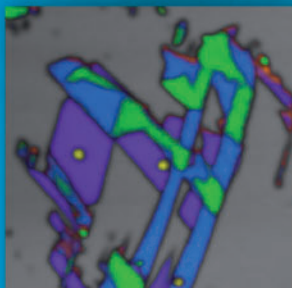
A Supplement To

Spectroscopy[®]

Solutions for Materials Analysis

June 2014 Volume 29 Number s6

www.spectroscopyonline.com



RAMAN TECHNOLOGY

for Today's Spectroscopists



Your Spectroscopy Partner

SPECTROMETERS | LASERS | TOTAL SOLUTIONS

We Offer a *Complete Ecosystem* of
Portable & Handheld Raman Analysis Instrumentation

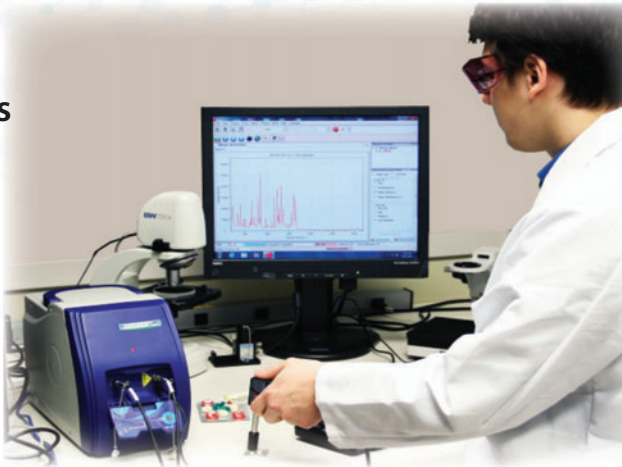
Schedule an appointment with us at
www.bwtek.com/livedemos
for a hands-on demo at an upcoming show

Either Domestic

Optics & Photonics
Booth #639
San Diego, CA

Or Abroad!

ICORS
Jena, Germany

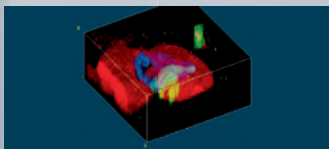


Let us run your sample.
We have the *solution* you need.

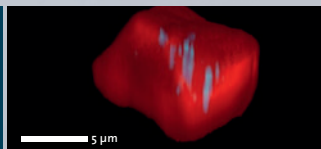
+1 (302) 368-7824 | www.bwtek.com

PIONEERS BY PROFESSION

The Bathyscaph Trieste arrived at the Earth's most extreme depth on 23. January 1960.



3D Raman image of a fluid inclusion in garnet



3D Raman image of a diamond inclusion (red) in quartz (black) with impurities (blue)

WITec's 3D Raman Imaging provides unprecedented depth and lateral resolution for chemical imaging down to the 200 nm diffraction limit. Our alpha300 and alpha500 series with optimized throughput and sensitivity establishes the benchmark in ultrafast spectra acquisition and low light-level microscopy.

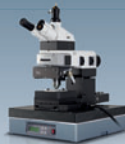
Achieve a deeper understanding than ever before with WITec's pioneering technology.



alpha300 R
First 3D confocal Raman imaging system



alpha500 AR
First automated Raman/AFM system for large samples



alpha300 SR
First SNOM system using patented cantilever sensors



PITCON® Editors' GOLD SERIES
Microscopy TODAY'S INNOVATION AWARD



Spectroscopy®

MANUSCRIPTS: To discuss possible article topics or obtain manuscript preparation guidelines, contact the editorial director at: (732) 346-3020, e-mail: lbush@advanstar.com. Publishers assume no responsibility for safety of artwork, photographs, or manuscripts. Every caution is taken to ensure accuracy, but publishers cannot accept responsibility for the information supplied herein or for any opinion expressed

CHANGE OF ADDRESS: Send change of address to Spectroscopy, P.O. Box 6196, Duluth, MN 55806-6196; provide old mailing label as well as new address; include ZIP or postal code. Allow 4-6 weeks for change. Alternately, go to the following URL for address changes or subscription renewal: <https://advanstar.replycentral.com/?PID=581>

RETURN ALL UNDELIVERABLE CANADIAN ADDRESSES TO: IMEX Global Solutions, P.O. Box 25542, London, ON N6C 6B2, CANADA. PUBLICATIONS MAIL AGREEMENT No.40612608

REPRINTS: Reprints of all articles in this issue and past issues are available (500 minimum). Call 877-652-5295 ext. 121 or e-mail bkolb@wrightsmedia.com. Outside US, UK, direct dial: 281-419-5725. Ext. 121

DIRECT LIST RENTAL: Contact Tamara Phillips, (440) 891-2773; e-mail: tphillips@advanstar.com

INTERNATIONAL LICENSING: Maureen Cannon, (440) 891-2742, fax: (440) 891-2650; e-mail: mcannon@advanstar.com



©2014 Advanstar Communications Inc. All rights reserved. No part of this publication may be reproduced or transmitted in any form or by any means, electronic or mechanical including by photocopy, recording, or information storage and retrieval without permission in writing from the publisher. Authorization to photocopy items for internal/educational or personal use, or the internal/educational or personal use of specific clients is granted by Advanstar Communications Inc. for libraries and other users registered with the Copyright Clearance Center, 222 Rosewood Dr. Danvers, MA 01923, 978-750-8400 fax 978-646-8700 or visit <http://www.copyright.com> online. For uses beyond those listed above, please direct your written request to Permission Dept. fax 440-756-5255 or email: mcannon@advanstar.com.

Advanstar Communications Inc. provides certain customer contact data (such as customers' names, addresses, phone numbers, and e-mail addresses) to third parties who wish to promote relevant products, services, and other opportunities that may be of interest to you. If you do not want Advanstar Communications Inc. to make your contact information available to third parties for marketing purposes, simply call toll-free 866-529-2922 between the hours of 7:30 a.m. and 5 p.m. CST and a customer service representative will assist you in removing your name from Advanstar's lists. Outside the U.S., please phone 218-740-6477.

Spectroscopy does not verify any claims or other information appearing in any of the advertisements contained in the publication, and cannot take responsibility for any losses or other damages incurred by readers in reliance of such content.

Spectroscopy welcomes unsolicited articles, manuscripts, photographs, illustrations and other materials but cannot be held responsible for their safekeeping or return.

To subscribe, call toll-free 888-527-7008. Outside the U.S. call 218-740-6477.

Advanstar Communications Inc. (www.advanstar.com) is a leading worldwide media company providing integrated marketing solutions for the Fashion, Life Sciences and Powersports industries. Advanstar serves business professionals and consumers in these industries with its portfolio of 91 events, 67 publications and directories, 150 electronic publications and Web sites, as well as educational and direct marketing products and services. Market leading brands and a commitment to delivering innovative, quality products and services enables Advanstar to "Connect Our Customers With Theirs." Advanstar has approximately 1000 employees and currently operates from multiple offices in North America and Europe.

PUBLISHING & SALES

485F US Highway One South, Suite 210, Iselin, NJ 08830
(732) 596-0276, Fax: (732) 647-1235

Michael J. Tessalone

Science Group Publisher, mtessalone@advanstar.com

Edward Fantuzzi

Publisher, efantuzzi@advanstar.com

Stephanie Shaffer

East Coast Sales Manager, sshaffer@advanstar.com
(774) 249-1890

Lizzy Thomas

Account Executive, ethomas@advanstar.com
(574) 276-2941

EDITORIAL

Laura Bush

Editorial Director, lbush@advanstar.com

Megan L'Heureux

Managing Editor, mlheureux@advanstar.com

Stephen A. Brown

Group Technical Editor, sbrowni@advanstar.com

Cindy Delonas

Associate Editor, cdelonas@advanstar.com

Dan Ward

Art Director, dward@media.advanstar.com

Anne Lavigne

Marketing Manager, alavigne@advanstar.com

Tamara Phillips

Direct List Rentals, tphillips@advanstar.com

Wright's Media

Reprints, bkolb@wrightsmedia.com

Maureen Cannon

Permissions, mcannon@advanstar.com

Jesse Singer

Production Manager, jsinger@media.advanstar.com

Jerry Xenos

Audience Development Manager, jxenos@advanstar.com

Gail Mantay

Audience Development Assistant Manager, gmantay@advanstar.com

Joe Loggia

Chief Executive Officer

Tom Florio

Chief Executive Officer Fashion Group, Executive Vice-President

Tom Ehardt

Executive Vice-President, Chief Administrative Officer & Chief Financial Officer

Georgiann DeCenzo

Executive Vice-President

Chris DeMoulin

Executive Vice-President

Rebecca Evangelou

Executive Vice-President, Business Systems

Julie Molleston

Executive Vice-President, Human Resources

Tracy Harris

Sr Vice-President

Dave Esole

Vice-President, General Manager Pharm/Science Group

Michael Bernstein

Vice-President, Legal

Francis Heid

Vice-President, Media Operations

Adele Hartwick

Vice-President, Treasurer & Controller

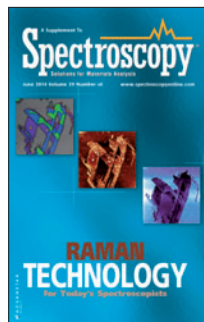
One Raman with 2 Lasers

for ultimate versatility and analytical power



Agility™ Dual-excitation Benchtop Raman System (any two lasers of 405, 532, 785 and 1064 nm)

- Transportable, Push-button Operation
- Automated laser switching
- Fluorescence-free Raman Spectra (by 1064 nm)
- Spectral library search and management
- Wireless remote control



RAMAN TECHNOLOGY FOR TODAY'S SPECTROSCOPISTS

JUNE 2014 VOLUME 29 ISSUE 6

Articles

8 High-Speed TERS Imaging: The Latest Achievements in nano-Raman Spectroscopy

E. Leroy, R. Lewandowska, O. Lancry, J. Schreiber, A Krayev, and S. Saunin

Developments in tip-enhanced Raman spectroscopy (TERS) that make nanoscale imaging of chemical and physical properties of graphene and other carbon species possible

24 Detection of Melamine and Other Harmful Food Contaminants Using Gold Nanoparticles, Surface-Enhanced Raman Scattering, and Raster Orbital Scanning

Yvette Mattley, Maja Sourdain, Derek Guenther, Cleo Harvey, and Adrian Guckian

The use of novel gold nanoparticles for surface-enhanced Raman spectroscopy (SERS) measurements with raster orbital scanning sampling is described for the detection of melamine and other food contaminants.

34 The Use of Portable and Handheld Raman Spectroscopy for Forensic Investigations

Katherine Bakeev and Robert Thomas

Portable and handheld Raman spectroscopy in the field of forensic science are discussed and illustrated with real-world examples.

42 Key Elements of Confocal Raman Microscopy for High-Resolution Imaging

Thomas Dieing, Marius Henrich, and Sonja Breuninger

The theoretical background of Raman imaging and the possibilities in practical applications are discussed.

Accelerate your work, visualize your answers

Whether developing new products, or troubleshooting and improving current processes, chances are Raman imaging can give you the edge you've been looking for. The Thermo Scientific™ DXR™xi Raman imaging microscope is a visually driven system that finds answers easily, with **all the performance you need and none of the learning curve**. You'll be an expert in Raman, covering more ground and ensuring critical processes, without missing a detail.

with smarter Raman imaging

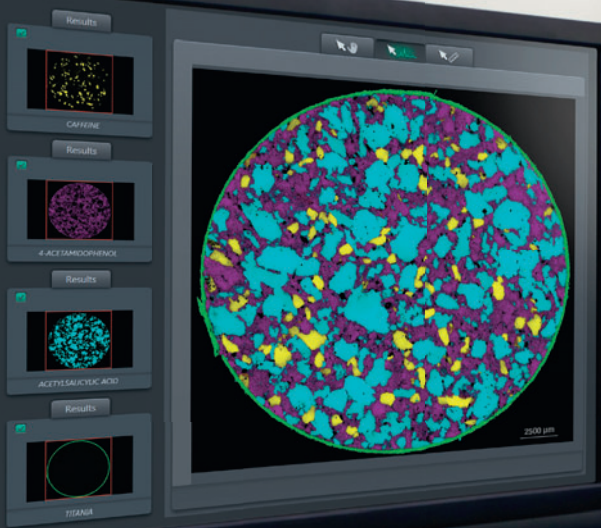
• see the big picture at thermoscientific.com/DXRxi



DXRxi Raman Imaging Microscope
High performance Raman imaging system in a complete, integrated package



Thermo Scientific™ OMNIC™xi Raman Imaging Software
Simple yet powerful image-centric software



High-Speed TERS Imaging: The Latest Achievements in nano-Raman Spectroscopy

This article presents developments in tip-enhanced Raman spectroscopy (TERS) that make possible nanoscale imaging of chemical and physical properties of graphene and other carbon species: Innovative integration of technologies brings high-throughput optics and high-resolution scanning for high-speed imaging without interferences between the techniques. Advances in near-field optical probes now provide reliable nanoscale spectroscopy solutions for academic and industrial researchers.

E. Leroy, R. Lewandowska, O. Lancry, J. Schreiber, A Krayev, and S. Saunin

Raman spectroscopy is a well-known technique to study carbon species. It provides a very specific signature for the two crystal configurations: diamond (cubic or octahedral) and graphite (hexagonal).

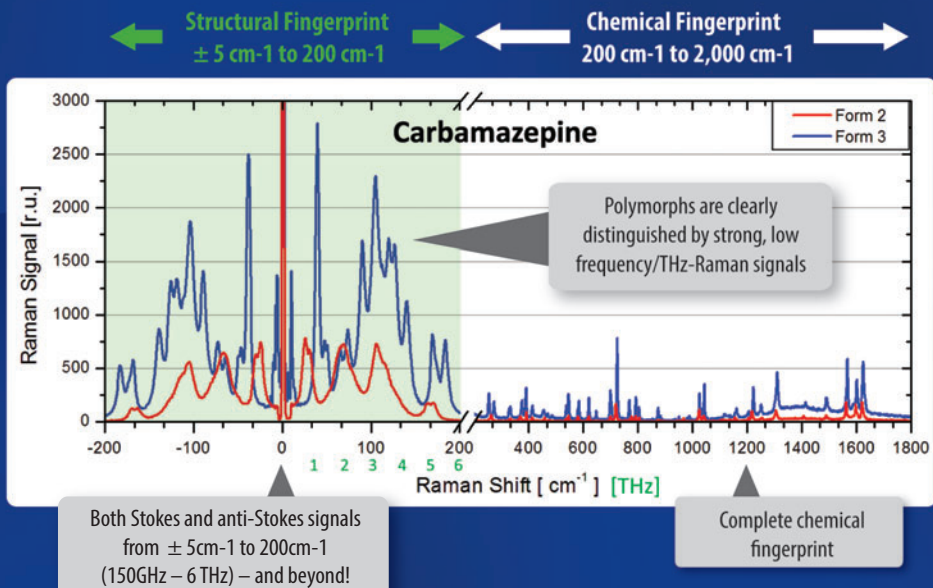
Because Raman microspectroscopy is an optical technique, its spatial resolution is limited by the laws of diffraction: As a rule of thumb, the spatial resolution of the technique is about half the wavelength of the exciting laser wavelength. This value depends on several factors besides the excitation wavelength, including the numerical aperture of the objective lens used; however, this approximation is convenient and easy to understand for the purpose of this discussion. With a red laser excitation, this is on the order of 300 nm.

Graphene flakes or coatings can be made quite large; however, other species of interest like single-wall carbon nanotubes (SWCNT) are typically in a diameter range of 1–3 nm, or two orders of magnitude smaller than the spatial resolution of the technique.

Raman spectroscopy brings chemical contrast for these species, and allows the determination of the diameter of a single wall carbon nanotube, or the number of layers in a multilayer graphene sample from the features present in the spectrum. Radial breathing mode frequency position is a good indicator of SWCNT diameter or the ratio and bandwidth of the G and two-dimensional (2D) bands in graphene are good indicators of the number of layers. However, the samples measured are generally not resolved spatially.

In contrast, scanning probe microscopy (SPM) and, in particular, the more popular technique atomic force microscopy (AFM) allow such materials to resolve spatially and provide even atomic-level resolution. Atomic resolution imaging of highly ordered pyrolytic graphite (HOPG) is a typical test for SPM calibration, using scanning tunneling mode (STM). The technique consists of scanning a very sharp probe over a sample and tracking the Z axis

Get the big picture with THz-Raman®



Ondax patented SureBlock™ THz-Raman® Spectroscopy Systems extend the reach of your Raman system down into the low frequency/THz regime, using only a visible or NIR laser. This unveils a secondary “structural fingerprint” that can be used to clearly differentiate polymorphs and synthetic pathways, or enhance forensic analysis of materials – all while maintaining the complete chemical fingerprint. Get the big picture with THz-Raman®!

SureBlock™ Ultra-low Frequency THz-Raman® Systems & Notch Filters



Compact benchtop, microscope and customized OEM solutions

SureLock™ Wavelength-stabilized Single Frequency Lasers



Stable, ultra-compact lasers from 405nm to 830nm

position via a feedback mechanism that depends on the mode used, to generate a topographic image. In STM, the feedback is done based on tunneling current intensity, and in AFM, a constant force is maintained between the probe and the sample by tracking the deflection of a laser on the back of a cantilever that holds the sharp probe. The cantilever bends according to its known mechanical properties that depend on size, shape, and material.

Beside topography, AFM can be used in a multitude of modes to obtain various physical properties. Looking at the way the probe interacts with the sample, it is possible to determine elasticity and plasticity of a material. Tracking the torsion of the level as it is scanned (lateral force) gives information about friction. Driving a current through a conductive probe, it is possible to obtain various electrical properties such as conductance, capacitance, and resistivity; surface potential is also determined by scanning above the surface. Using a magnetized probe, magnetic studies can be performed at various heights from the surface.

SPM and, in particular, AFM are very versatile techniques to image a multitude of physical properties, however, neither technique provides chemical specificity (except in the case of the use of functionalized probes designed for very specific chemical bonding).

The interest for combining the two techniques is obvious: Obtaining physical properties and chemical specificity of the same location, ideally simultaneously, without having to move the sample or find the location of interest each time is a huge time saver when studying nanomaterials.

The combination of the two techniques is in itself interesting, but fur-

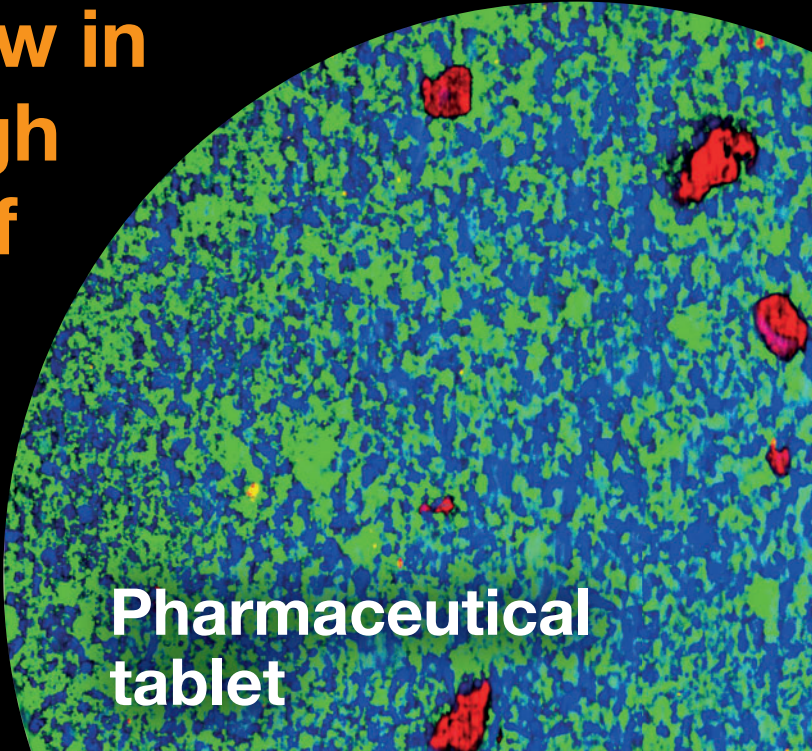
thermore reducing the spatial resolution gap between the two techniques is of the highest interest. This is where tip-enhanced Raman spectroscopy (TERS) comes into play.

TERS takes advantage of the enhancement of several orders of magnitude observed in techniques like surface-enhanced Raman spectroscopy (SERS), confining this enhancement at the tip of a specially crafted probe that acts as a plasmonic antenna. The result of this confined resonance is an extremely localized enhancement of the Raman signal in the very close vicinity of the tip of the probe, generally no further than 10 nm. A laser beam matching the probe's plasmonic excitation range is focused on the probe to produce the local enhancement. The focused laser beam is of course following the same diffraction rules mentioned above, and illuminates a field much larger than the probe tip radius, potentially exciting a far-field (diffraction limited) Raman signal, while the enhanced signal is localized just under the probe generating the near-field Raman signal. The ratio of the volumes involved in each case is also several orders of magnitude, so the ability to detect the near-field Raman signal is extremely dependent on the probe quality and its enhancement efficiency.

SWCNTs have been studied in the past with TERS, most often performing line scans (1) and a few produced images (2).

The novelty presented here and demonstrated in the experimental measurement of graphene oxide and single-wall carbon nanotube samples is in the combination of the techniques into an instrument in such an efficient manner that it is possible to obtain reliable enhancement and stable alignment to perform

Raman images: now in high def



Pharmaceutical tablet



Clear, crisp Raman images

Renishaw's new WiRE 4 Raman software enables you to capture and review very large Raman datasets and produce high definition Raman images.

These can be as large and crisp as you like.

Apply innovation
Improve your images

TERS imaging with very short acquisition times, which in turns frees the technique from the need to subtract far-field from near field and from potential drift issues inherent to the SPM technology.

Experimental

The experimental setup consists of a nano-Raman integrated system from Horiba Scientific and AIST-NT Inc. A SmartSPM scanning probe microscope (AIST-NT Inc.) with an Omegascope microscope was used for top-down and oblique illumination and collection. The microscope is integrated with a Horiba XploRA Plus Raman microspectrometer (or it can eventually also be fitted with a Horiba Labram HR Evolution spectrometer for added functionalities). In this configuration, the spectrometer was fitted with an electron-multiplying charge-coupled device (CCD) detector for fast data acquisition.

In this work, different samples were prepared. The first set of images generated consists of colocalized confocal Raman and AFM imaging of graphene flakes. The sample is mechanically exfoliated graphene deposited on a silicon substrate using the widely referenced transparent adhesive tape method. In this case, a 532-nm laser was used for Raman spectroscopy, with a power of 25 mW at the sample. Acquisition time for the image shown is about 7 ms per point. The area measured is $35\ \mu\text{m} \times 35\ \mu\text{m}$.

The second sample was prepared by dispersion of a graphene oxide and carbon nanotube mixture from solution spin-coated on a flame-annealed 5 mm \times 5 mm gold substrate. Spin-coat time and solution concentration were adjusted to obtain a distribution of about one or two tubes and one or two graphene oxide flakes per square micrometer, so

as to easily find an area of interest while avoiding aggregation of nanotubes. This second sample was measured with AFM first to verify the proper distribution of the two carbon species, and then it was imaged with TERS. The laser wavelength used was 638 nm. The laser output power is typically 24 mW, but only a few hundred microwatts to about 6 mW were used in this case.

In performing AFM-Raman imaging or TERS, a critical step consists of making sure the Raman laser is properly aligned with the probe. In AFM-Raman imaging, an offset in the order of the spatial resolution of the Raman technique is acceptable, but it is much less forgiving when performing TERS measurements. For this purpose, the Raman laser is aligned using a piezo-driven objective scanner, with closed-loop feedback, similar to the scanning probe microscope sample scanner. This device ensures the long term stability of the alignment. Since it displaces the objective lens only, it does not introduce any additional optical component, guaranteeing maximum throughput, and since it is effectively moving the last piece of optic before the sample, the beam pathlength is minimized for best stability.

Another notable feature of the setup is the use of an infrared diode for AFM feedback. Most SPM systems use a diode in the red or near-infrared (NIR) range, potentially interfering with the collection of the Raman signal in those spectral ranges. Avoiding this range is especially critical for AFM-TERS, using an AFM cantilever, as the most stable probes today are made out of gold whose plasmon resonance frequency is in the red region. Using an infrared feedback diode ensures there is no interference with the optical

Chem Logix™

RAISING THE BAR IN RAMAN SPECTROSCOPY

Introducing TSI's full line of high-performance, easy-to-use Raman spectrometers boasting:

- + Hand held, portable, and laboratory bench top instruments
- + Research-grade performance at an affordable price
- + Fast material identification with shortest sample times
- + Repeatable instrument to instrument, database transferable across all platforms
- + Excellent fluorescence rejection
- + The right material ID the first time

Contact TSI for the right raman instrument for your needs or **visit: www.tsi.com/RAMAN**



UNDERSTANDING, ACCELERATED



spectroscopy system. Furthermore, the AFM diode is not visible in the video image and does not tend to excite fluorescence in the sample, allowing artifact-free Raman measurements.

The dual microscope setup brings a few advantages: It allows top down measurements, which makes simultaneous and colocalized measurement of AFM images and spontaneous Raman hyperspectral images possible, with high spatial resolution. The top-down approach is best for high spatial resolution on opaque samples in spontaneous Raman measurement mode because the laser can be tightly focused with a high numerical aperture (NA) objective lens (0.7 NA in our case when simultaneous AFM and Raman measurements are made, and up to 1.4 NA with oil immersion objectives when the AFM probe is removed for Raman measurements only).

The oblique (or side) illumination scheme is not ideal for spontaneous Raman measurement as the laser spot is focused at a 60° angle and, therefore, is not Gaussian but elliptical. Spatial resolution is degraded, but this is the preferred mode of illumination for tip-enhanced Raman measurements because it allows better illumination of the apex of the probe, while providing proper alignment of the electromagnetic field of the incident laser beam with the axis of the plasmonic probe without the need for further polarization conditioning of the beam.

It has been shown in simulation that this illumination scheme also brings the highest surface plasmon resonance enhancement of the Raman signal and that it is then localized directly under the apex of the probe (3), as opposed to the side when polarization orientation is not optimized. This confinement of the Raman enhancement below the probe

apex, providing the probe has a high enhancement contrast, is what brings spatial resolution of the near-field Raman signal down to about 10 nm, well below the actual probe apex radius, which is typically in the order of 30 nm.

The probes used are commercially available probes manufactured by Horiba and made from etched gold wire following a process adapted from the original publication by Bin Ren and colleagues (4) and improved by the Laboratoire de Physique des Interfaces et des Couches Minces (LPICM) laboratory of the Ecole Polytechnique in France. The probes are mounted on a tuning fork for this experiment.

TERS imaging has been considered to be very complex because of the many factors that may affect the measurement. The novelty in the equipment primarily consists in the use of efficient, reliable probes developed in collaboration with academic researchers, in the optimization of the optical path and alignment technology to reduce drift, and in the integrated control of the different hardware components to improve data acquisition speed, which in turn reduces potential drift issues.

In the setup described, the measurement time is typically 5–100 ms. This is possible thanks to the use of the electron multiplying charge coupled device (EMCCD) detector that allows detection of signals below the read noise of the device. Such a detector is very popular in fluorescence microscopy for this capability; however, in spectroscopy it has a few trade-offs and is essentially useful to accelerate acquisition. EMCCD technology adds a gain factor called *electron-multiplier* before the electrical signal is converted into a digital signal through the analog-to-digital converter (ADC).

Extreme High Sensitivity in Raman



Raman spectroscopy is a precise and versatile measurement tool. It only has one downside: Raman signals are difficult to detect due to the required combination of high resolution with high sensitivity.

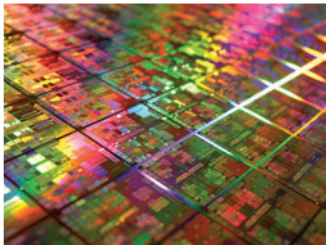
The AvaRaman-XHS series spectrometers solve this problem by offering extremely high sensitivity combined with high resolution. Up to six times the sensitivity of a comparable priced Raman systems can be achieved. Measurements can be done faster and more precise.



By redesigning the optical bench and especially the light entrance, more than 95% of the light coming out of the fiber optic cable reaches the detector. The standard solution with an entrance slit only sees 15 percent of the photons reach the CCD.

AvaRaman-XHS-TEC series spectrometers have a three-stage Peltier cooling systems, which provides ΔT down to -30°C cooling to ambient for superior dark noise reduction, keeping the detector at a steady 5°C . Thanks to the PID controller, this temperature is stable within a 0.1°C bandwidth.

For applications requiring less sensitivity, the current AvaRaman systems are an ideal cost-effective alternative.



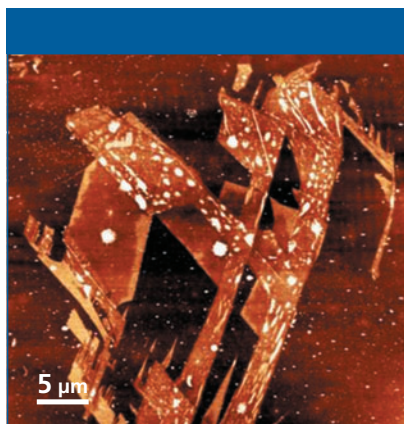


Figure 1: AFM topography of a set of graphene flakes of different thickness.

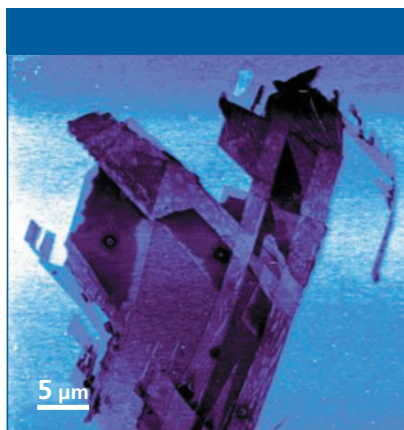


Figure 2: Surface potential difference image of the graphene flake sample. This technique, also referenced to as Kelvin probe microscopy, provides information about the electronic state on the surface.

This, in effect, allows the detection of signals below the read noise, which is the noise produced by the ADC while converting. However, this also has the effect of dramatically reducing dynamic range because any signal above the read noise is enhanced to levels bringing it closer to the saturation level of the ADC. This gain process does not effectively

bring any advantage when the signal is already above the read noise level. Considering a Raman signal with a signal to noise ratio of 100:1 obtained in 1 s, if we decrease integration time to such a level that the signal is below the read noise, in our case 10 ms for example, the electron-multiplier gain can now bring this signal above the read noise level and enhance it to regain a readable spectrum with enough contrast to extract information about the bands of interest and generate an image rendering based on this information.

However, using the electron-multiplier gain does not produce high quality spectra. Longer acquisition times or the accumulation of multiple spectra is usually necessary to obtain data that can be used for precise spectral analysis. The technique, however, can image and locate areas of interest quickly, which can then be investigated further.

Results and Discussion

The first measurements consist of the analysis of graphene flakes of different size and thickness. Figure 1 shows a topography image of the sample, which gives information on the graphene flake thickness. Even though the topography image can help determine the presence of single-layer or multiple-layer graphene, the roughness of the substrate itself, which can be much larger than the single atomic step of carbon, can understandably interfere with this measurement.

Figure 2 is the surface potential image of the sample, also known as Kelvin probe force microscopy (KPFM), and provides information about the electronic state of the surface of the sample.

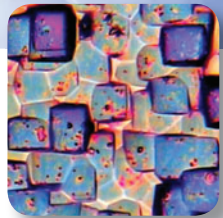
Figure 3 shows a false color composite Raman image of the sample generated

SENTERRA

The **only** Raman microscope with permanent wavelength calibration



- High wavenumber accuracy (Sure_Cal®)
- All-in-one, compact, flexible
- Concave Rubberband Correction for smart removal of fluorescence background
- High performance confocal design with FlexFocus™
- Up to four excitation lasers



The SENTERRA is a revolution in dispersive Raman spectroscopy. In contrast to conventional instrumentation no calibration of the wavelength scale is required as the system is permanently calibrated with extremely high accuracy.

As this system further provides a very high sensitivity even used in confocal mode, the SENTERRA is the perfect Raman microscope for a very broad range of applications.

Contact us for more details:
www.bruker.com/senterra

Bruker Optics Inc.
Billerica, MA · USA
Phone +1 (978) 439-9899
Fax +1 (978) 663-9177
info@brukeroptics.com

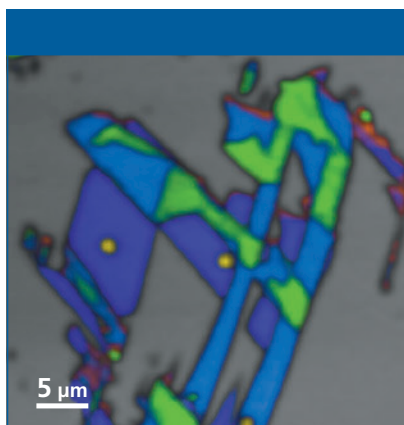


Figure 3: False color image generated from classical least square deconvolution of the Raman hyperspectral image. The silicon substrate is shown in gray, single-layer graphene is purple, two-layer graphene is blue, three-layer-graphene is green, amorphous carbon is yellow, and defective graphene is orange, primarily concentrated on the edges of the flakes.

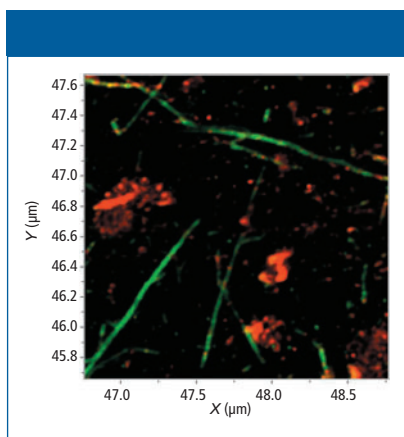


Figure 4: Image of carbon nanotubes (green) and graphene oxide (red) on gold substrate obtained in tuning fork mode. This 200×200 point, $2 \times 2 \mu\text{m}$ image was obtained in 8 min with spatial resolution of 10 nm.

from classical least squares deconvolution of the Raman hyperspectral data cube. The silicon substrate is shown in

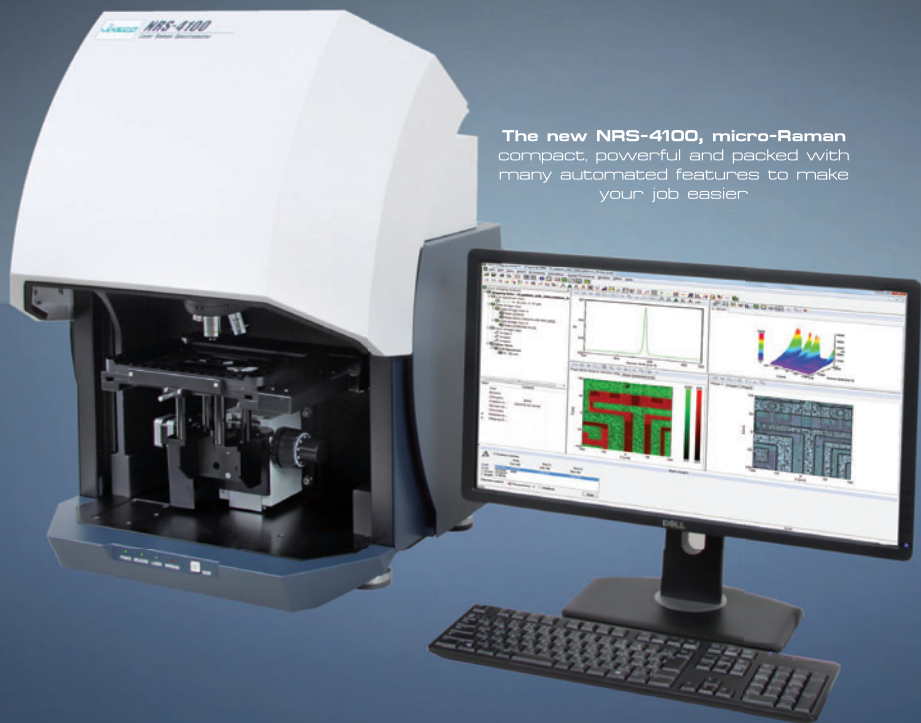
grey, single-layer graphene is shown in purple, two-layer graphene is shown in blue, three-layer graphene is shown in green, amorphous carbon is shown in yellow on a couple spots (this is believed to be from over-exposure with the Raman laser), and defective graphene is shown in orange, which is primarily concentrated on the edges of the flakes.

In this example, it can be seen that the Raman image is of lower spatial resolution than the AFM images even though the number of data points is equivalent as the topography and Raman images were generated simultaneously. The KPFM image can be generated in one pass, but it is most often generated in two passes to avoid cross-talk, so this image was generated separately.

It is undeniable in these images that complementary information is obtained, demonstrating the usefulness of the technique. The topography can be correlated closely to the Raman spectral information, which provides clear confirmation of the graphene flake thickness.

Raman spectroscopy provides more detailed information on the chemical structure of the graphene and especially the presence of defects, which are more commonly found on the edges of the flakes. This can easily be explained by the fact that the ordered hexagonal lattice is indeed disrupted at the edge.

The ability to generate multiple images simultaneously is common in scanning probe microscopy where electrical signals are measured, however, acquiring Raman spectra calls for a very different approach and the use of a CCD detector, which tends to be much slower. The ability of the equipment to perform both simultaneously ensures that the data obtained effectively come from the same location.



The new NRS-4100, micro-Raman compact, powerful and packed with many automated features to make your job easier

With the 457nm high output laser - this might be the only system you ever need! High power, Excellent spatial resolution and spectroscopy from 8000 to 100 cm^{-1} (or 50 cm^{-1} optional)

If you want to use the conventional combination of 532/785nm, we've got that covered as well (and up to 1064nm).

- JASCO patented Fluorescence Correction
- Auto-alignment of the optical path and laser alignment
- Automatic exchange laser and rejection filter for up to 3 lasers
- Automatic sample identification
- Real-time laser spot observation
- Real-time assist - makes sure you get the best measurement
- JASCO Spectra Manager II for imaging and spectroscopy

If you want to find out why so many laboratories are choosing JASCO for their RAMAN requirements, come and check us out at:

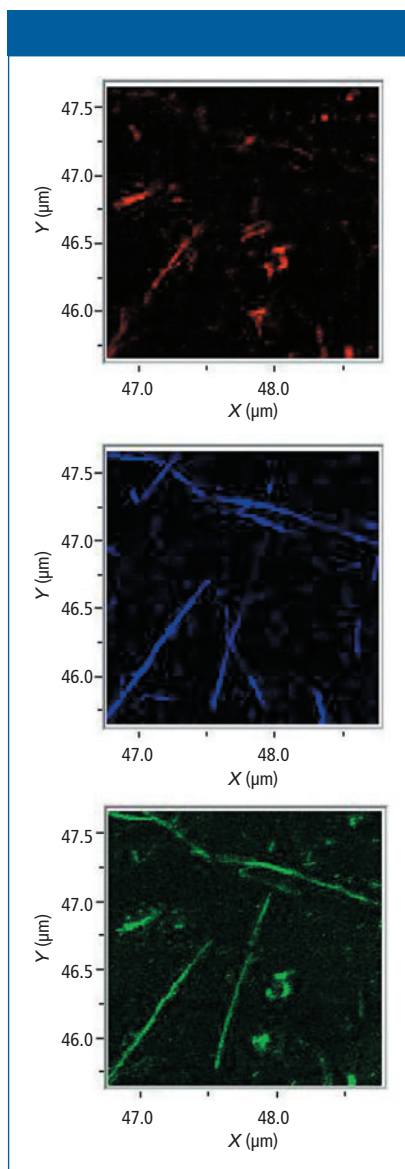


Figure 5: Images of the D band (red), G band (green), and 2D band (blue) of the graphene oxide and carbon nanotubes sample. The nanotubes show strong typical G and 2D bands while graphene oxide shows no 2D band but high disorder (D band). Some nanotubes show higher disorder than others in the presence of a D band as well.

Because we are using a sample scanner, effectively moving the sample in all three dimensions (X , Y , and Z) the sample is moved to track the cantilever position, as opposed to adjusting the cantilever position to track the sample. This has an added advantage because of the fact that the Raman laser, which is also aligned on the probe, remains in focus on the sample at all times, no matter what the height of the topography is, essentially acting as a real-time autofocus. This is not evident in the sample measured in this work, but becomes critical when looking at samples with topography in the several micrometer range: Because of the confocal nature of the system, the depth of field is only on the order of a micrometer, and without tracking the sample position, only a thin Z slice of the sample would be measured properly.

The next experiment demonstrates Raman imaging at high speed with nanoscale resolution.

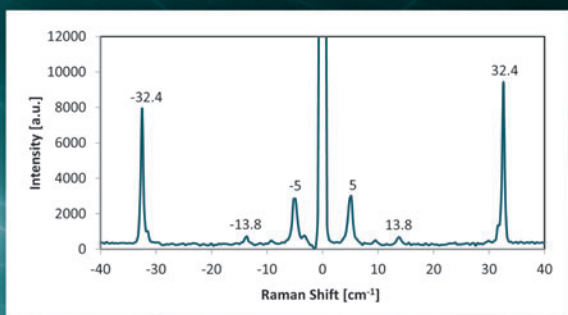
The TERS image in Figure 4 is 200×200 points mapped over a $2 \mu\text{m} \times 2 \mu\text{m}$ area and was obtained with 12 ms acquisition time per spectrum, yielding 40,000 points in about 8 min. It has been deconvoluted with a classical least squares method to extract the three components of interest: the graphene oxide, the carbon nanotubes, and the background signatures, shown in false colors in red, green, and black, respectively.

This method yields the most contrast when the goal is to differentiate the different carbon species, but misses the information contained in the specific bands of interest. In particular, the D band (around 1330 cm^{-1}) is typically associated with disorder in the hexagonal carbon structure.

Figure 5 shows the individual images generated by rendering intensity of the

Ultra-Low Frequency Raman Spectroscopy

"Extend your Raman system into THz frequency range ($5\text{-}200\text{ cm}^{-1}$)"



Raman spectrum of MoS_2 flakes measured at 633 nm with BragGrate™ Notch filters and single stage spectrometer

(data courtesy of: P. H. Tan, State Key Laboratory of SL and Microstr., Institute of Semiconductors, CAS, Beijing, P. R. China)

BragGrate™ Bandpass and Notch Filters

Spectral and spatial laser line cleaning filters and ultra-narrow line notch filters for low frequency Raman Spectroscopy



488 nm 633 nm
514 nm 785 nm
532 nm 1064 nm

- Frequencies below 10 cm^{-1} with single stage spectrometer
- Stokes and anti-Stokes Raman bands
- Unlimited optical life-time
- Custom wavelengths in range 400–2000 nm

OptiGRATE
HIGH EFFICIENCY FOR HIGH POWER

+1 (407) 542-7704
info@optigrate.com
www.optigrate.com

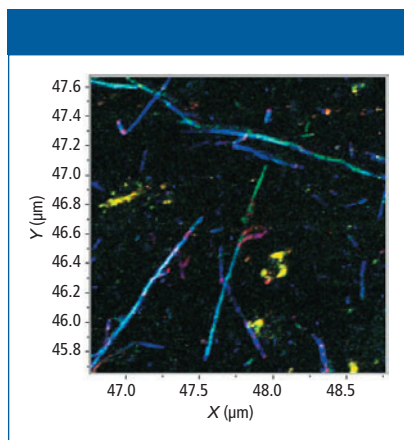


Figure 6: Overlay of the three images from Figure 2.

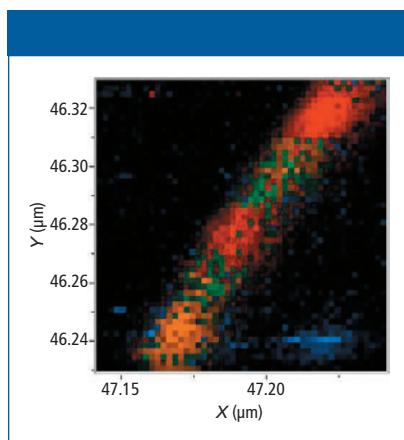


Figure 7: Close-up image of a nanotube. The image is 100×100 nm with 2-nm steps (50×50 points, obtained in 40 s).

specific carbon bands. The D band is shown in red, the G band is shown in green, and the 2D band is shown in blue.

Graphene oxide is highly disordered and shows strong D band and G band typical of the graphitic structure. Carbon nanotubes show strong G and 2D bands as is typical, but also show some presence of a D band in some areas, indicating the presence of defects in the tube structure.

Figure 6 shows the overlay of all three colors, bringing graphene oxide in yellow (mixture of red and green) and carbon nanotubes mostly in various shades of blue indicative of the defective structure.

In Figure 7, a close-up image was generated. It is 50×50 points, 2-nm steps, and was obtained in 40 s. Figure 8 shows the corresponding spectra extracted by classical least squares deconvolution of the image in Figure 7.

This image is a good illustration of the variability of the nanotube chemical structure at the nanoscale which is impossible to resolve with standard confocal Raman imaging, and which cannot be extracted by typical SPM techniques. In these spectra, we observe a range in level of disorder in the carbon material from the red spectrum (low disorder, low intensity of D band) to green to orange (higher level of disorder, highest intensity of D band).

Conclusions

This work does not pretend to expose novel science or understanding of AFM-Raman and TERS, but aims at demonstrating the current capabilities available today. Imaging carbon nanotubes with TERS has been done before, however, there are very few publications demonstrating this capability on a strictly commercial instrument. The leading groups in TERS have demonstrated the capabilities of the technique for several years now, yet even though many of the setups used are built from commercially available systems, almost all have been modified for the purpose of developing the technique.

Researchers wanting to approach this technique today are faced with the need to account for many subtle, but important modifications to get results.

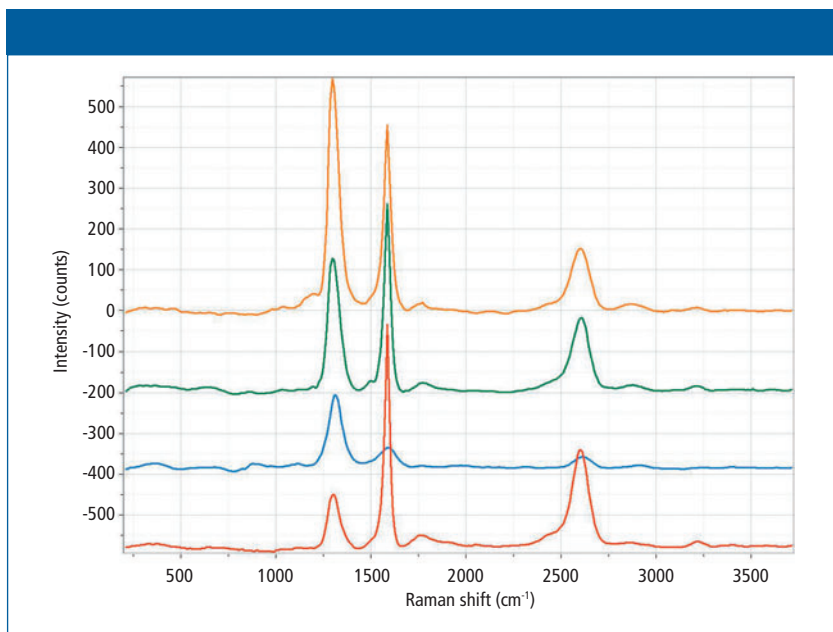


Figure 8: Reference spectra for classical least squares deconvolution of the image in Figure 7.

In this work, we presented the capabilities of a strictly commercial instrument designed for purpose. Evidently, one of the key factors in successful TERS is the availability of suitable and efficient probes. With the development of its own probe manufacturing in collaboration with academia, a complete solution for TERS is now commercially available. Furthermore, many of the limitations that make AFM-TERS difficult have been removed, and the platform is ready to use such probes when they become available, without the risk of optical interference.

In the past, TERS was not a technique reserved for the faint-hearted; this work shows that it is now easier than ever to get results quickly and reliably. Many years of experience have been put into perfecting the instrumentation. Now, this experience is available and application development is the focus of research.

References

- (1) G. Picardi, M. Chaigneau, and R. Ossikovski, *Chem. Phys. Lett.* **469**, 161 (2009).
- (2) L.G. Cançado, A. Hartschuh, and L. Novotny. *J. Raman Spectrosc.* **40**(10), 1420–1426 (2009).
- (3) A. Downes, *J. Phys. Chem. B* **110**, 6692 (2006).
- (4) B. Ren, G. Picardi, and B. Pettinger, *Rev. Sci. Instrum.* **75**, 837 (2004).

E. Leroy, R. Lewandowska, O. Lancry, and J. Schreiber are with Horiba Scientific in Palaiseau, France. **A. Krayev and S. Saunin** are with AIST-NT Inc., in Novato, California.

Direct correspondence to:

Emmanuel.leroy@horiba.com ■

For more information on this topic,
please visit our homepage at:
www.spectroscopyonline.com

Detection of Melamine and Other Harmful Food Contaminants Using Gold Nanoparticles, Surface-Enhanced Raman Scattering, and Raster Orbital Scanning

Melamine is a dangerous substance when it is used to increase the apparent protein content of food. In this article, the use of novel gold nanoparticles for surface-enhanced Raman spectroscopy (SERS) measurements with raster orbital scanning sampling is described for the detection of melamine and other food contaminants. Although silver nanoparticles are often used for melamine SERS measurements, gold nanoparticles are more stable with less stringent requirements for storage and handling. Gold SERS substrates can also be used for the detection of other harmful food additives and adulterants, including antifungal dyes, antibiotics, and pesticides.

Yvette Mattley, Maja Sourdain, Derek Guenther, Cleo Harvey, and Adrian Guckian

Food safety is a global concern that has spawned rigorous guidelines and numerous regulatory agencies to protect consumers from both harm and fraud (1). Widespread illness and even death have resulted from the adulteration of food with compounds like melamine, which are added to ensure substandard foods meet dietary guidelines. Trace contaminants and residues from pesticides and antifungal agents used in the growth, processing, and storage of food products have been shown to be toxic to humans with impacts ranging from digestive problems to death. Counterfeit food products deceive consumers, risking their health while emptying their wallets. It is these ongoing deceptive and

dangerous practices and the widespread illness and economic impact they have caused that have driven the establishment of strict food safety regulations and the need for careful food inspection.

Consumers rely on government scrutiny and oversight for protection from dangerous food additives and contaminants. The use of melamine and its derivative, cyanuric acid, have invited scrutiny and inspired tighter regulation of fungicides, pesticides, and antibiotics used for crop protection. The antifungal agents crystal violet and malachite green are inexpensive and effective against fungal and parasite infections in fish, but are not approved for use in aquaculture because of their mutagenic impact

on humans. The fungicide thiram is used to protect crops from deterioration both before and after harvest, but has high enough toxicity that it requires protective clothing for handling. The broad-spectrum antibiotic chloramphenicol is banned for food use and is tightly regulated to avoid toxicity and the potential for the creation of antibiotic-resistant bacteria. These compounds and many others have documented health and safety concerns requiring regulation and inspection of food products.

With the potential for serious health and economic effects, there is a need for a rapid, low cost, and sensitive technique to detect and identify harmful food contaminants. Although there are a variety of methods and techniques now available for the identification and quantification of these potentially harmful compounds, these techniques (high performance liquid chromatography–mass spectrometry [HPLC–MS], gas chromatography–mass spectrometry [GC–MS], and ion-mobility spectrometry [IMS]) are often expensive, time- and labor-intensive measurements requiring significant sample preparation and highly trained personnel to administer. For a viable, commercial application, a method is needed that requires little to no sample preparation, is applicable to a range of food contaminants, and can provide fast, accurate identification and quantification. Surface-enhanced Raman spectroscopy (SERS) meets these requirements and is a good option for the detection of food contaminants and additives.

Raman spectroscopy is a high-resolution, vibrational spectroscopic technique in which each molecule produces a unique spectral “fingerprint” that can be used to identify and differentiate it from other sample components. Recent advances in lasers, detectors, and opti-

cal filter technologies have lowered costs and enabled considerable downsizing of Raman instrumentation such that the technology is more accessible and field deployment is now feasible. As a detection technology, Raman spectroscopy (2) has gained increasing interest because the Raman band frequencies relate to chemical bonding in the compound to be identified. This chemical specificity gives detection by Raman spectroscopy a distinct advantage. Different compounds have unique Raman fingerprints that can be used to identify them.

The major drawback of Raman spectroscopy is the low cross-section (2) of the spontaneous Raman scattering, which affects the detection of substances at trace level. This small scattering cross-section results in lower Raman signals and makes detection and identification difficult for compounds like food contaminants and additives that are present at low concentrations. In 1977, a technique to overcome this limitation was demonstrated when the compound of interest was placed on a roughened noble-metal substrate. The result was a significant enhancement in the magnitude of the Raman scattering signal (3). This process is known as *surface-enhanced Raman scattering* (4,5).

The enhanced sensitivity achievable with SERS makes it a viable option for the detection of food contaminants often present at trace levels. SERS is a variation of conventional Raman spectroscopy whereby analytes are adsorbed onto a noble metal (typically gold or silver) covered surface before analysis. Through a combination of chemical and electromagnetic effects, the Raman signal intensity is significantly “enhanced” when measured from SERS substrates fabricated from these noble metals. In very specific cases, detection at the sin-

gle-molecule level has even been demonstrated (6,7). The combination of signal enhancement and chemical specificity make SERS a good candidate for the sensitive and selective identification of compounds including harmful food contaminants and additives (8,9).

Since the early days of SERS, gold (Au) and silver (Ag) have been widely used as SERS substrates because of their strong SERS activity (10). The use of these metals has advanced with the development of nanoscience and nanotechnology, which give researchers the ability to control the shape, size, and composition of silver and gold nanoparticles. As a result, silver and gold are the most widely used SERS substrates. Theoretical calculations indicate that the Raman enhancement of a single gold nanoparticle is about 10^3 – 10^4 with enhancement for a single silver nanoparticle as high as 10^6 – 10^7 (11).

In this paper, we describe the novel combination of gold substrates and raster orbital scanning (ROS) for the detection of melamine and other harmful food additives and contaminants. Data illustrating the increased stability of the gold substrates relative to silver substrates are shown along with the enhancement in signal achieved with ROS sampling versus traditional Raman sampling. The broad applicability of the gold SERS substrates is also shown for several other food contaminants.

Although melamine is typically detected using silver SERS substrates with 532-nm laser excitation, we used gold substrates with 785-nm laser excitation for our measurements. Although melamine binds well to silver, one of the limitations of the silver substrates is a shorter lifetime, requiring modified atmospheric packing of the substrates and special storage and handling conditions

(12,13). Gold, on the other hand, ages much more slowly with better stability than silver (14,15). This increased stability and longer lifetime are why we used gold substrates even though melamine binds better to silver. Gold also has the added benefit of working with a broader range of harmful food additives and contaminants.

When the more stable gold SERS substrates are combined with an ROS Raman sampling technique, the result is a rapid, sensitive method for detecting several regulated or banned food additives and contaminants. ROS combines the resolution and power achieved with a tightly focused laser spot with the sensitivity of sampling over a large sample area. By rastering the laser spot over a large sample area, there is a higher probability of measuring spectra from SERS hotspots (localized regions of Raman signal enhancement) dispersed on the substrate. This results in higher sensitivity than with traditional Raman sampling where the laser is focused on a single location on the substrate. This is especially important with SERS substrates, in which the density and coverage of nanoparticles on the substrate can vary from location to location. Not only does ROS overcome this challenge of working with SERS substrates, it also provides a lower average laser power at the substrate and reduces the possibility for substrate or sample damage during exposure to the tightly focused laser.

Experimental

Silver and gold nanoparticles were inkjet printed on cellulose substrates. For substrate aging studies, melamine was tested on the day of printing and up to one week after printing. Measurements were made by drop casting 12 μ L of the com-

pounds suspended in various solvents to the printed SERS substrates mounted on standard glass microscope slides.

The substrates were interrogated with either an IDRaman reader integrated Raman system from Ocean Optics with 785-nm laser excitation and ROS sampling (IDRaman reader) or with a modular Raman system from Ocean Optics comprising a QE *Pro* spectrometer configured for 785-nm Raman measurements (QE *Pro* Raman), a 785-nm laser for excitation (LASER-785), and a Raman probe for detection (RIP-RPB-785). Typical acquisition parameters were three scans to average and a 1-s integration time. Data were acquired using OceanView software (Ocean Optics).

In all the plots presented, the spectra were adjusted for an appropriate baseline to enable comparison of peak height values. A Raman-inactive area of the spectrum was determined for each analyte, and the average value across that region was subtracted from the rest of the spectrum. This achieves a baseline correction that accounts for the noise seen in the raw spectrum. The spectra reported are raw spectra that have been baseline corrected.

The observed shifts in the assigned peaks for the analytes could result from a variety of factors. It is known that differences in solvents and, more importantly, physical features in SERS substrates will cause the observed peaks to change. These changes explain any variation in peak assignment when compared to reference literature.

Results and Discussion

Impact of Substrate Aging

To demonstrate the impact of substrate aging on the SERS detection of melamine, silver and gold nanoparticles were inkjet printed on cellulose substrates. Melamine

at 1×10^{-2} M concentration in water was drop casted to the substrates and Raman spectra were measured on the day of printing and 24 h after printing.

The Raman spectra measured with the modular Raman system using traditional Raman sampling for melamine on a silver substrate are shown in Figure 1. Note the characteristic peak for melamine near 700 cm^{-1} in the spectrum measured just after the substrate was printed (day 0). Deterioration of the silver substrate is observed by the loss of this peak in the Raman spectrum measured 24 h after the substrate was printed (day 1). The silver substrate degraded significantly within 24 h of printing, resulting in an inability to detect melamine with this aged substrate.

When a gold substrate is used to measure the same melamine solution, the improvement in stability is dramatic. As shown in Figure 2, the characteristic melamine peak is still observed one week after the gold substrate was printed. Additional studies (data not shown) have demonstrated even longer stability with measurements made with gold substrates more than 60 days after printing. This increased stability makes gold substrates easier to work with than silver substrates and more suitable for use in a commercial application.

The improvement in the SERS measurements for melamine is even better when the excellent stability of the gold substrates is combined with the ROS sampling technique. When the relative intensity of the Raman peaks for melamine in Figure 2 is compared to the relative intensity of the melamine peaks in Figure 3, the signal measured with ROS sampling (Figure 3) is almost two times the relative intensity of the signal measured with traditional Raman sam-

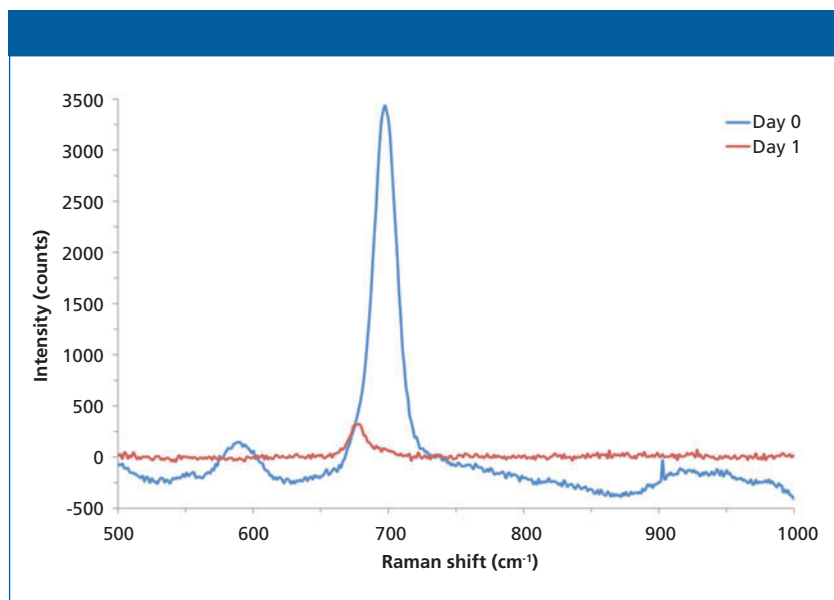


Figure 1: Aging of inkjet-printed silver SERS substrates 24 h after printing: Raman spectra for 1×10^{-2} M melamine in water measured using traditional Raman sampling.

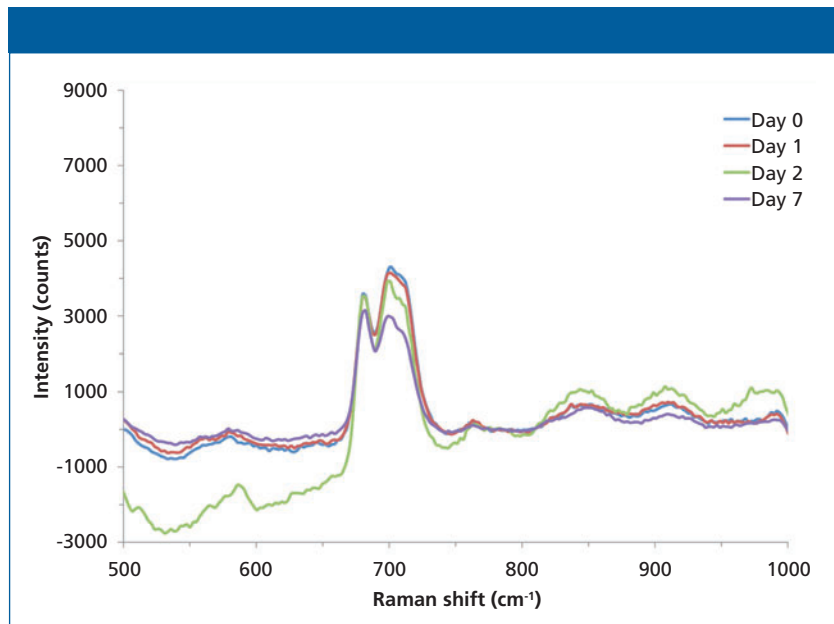


Figure 2: Improved substrate stability with inkjet-printed gold SERS substrates one week after printing: Raman spectra for 1×10^{-2} M melamine in water measured using traditional Raman sampling.

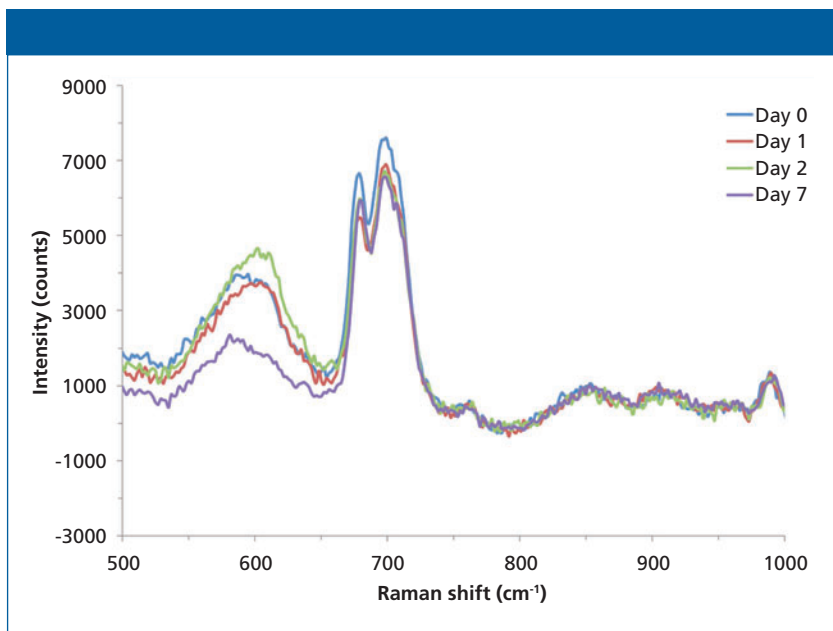


Figure 3: Improvement in Raman signal with ROS sampling of inkjet-printed gold SERS substrates: Raman spectra for 1×10^{-2} M melamine in water measured using ROS sampling.

pling (Figure 2). This increase in Raman intensity measured using ROS sampling clearly demonstrates the dramatic improvement in sensitivity achieved with ROS when a larger area of the SERS substrate is sampled. By sampling a larger surface area, more Raman hotspots are measured leading to improved sensitivity and the possibility to detect even lower concentrations of melamine or other food contaminants and additives.

Detection of Other Compounds of Food Safety Concern

As demonstrated in Figures 4–7, in addition to their stability, another advantage of gold substrates is that they can be used for the detection and discrimination of a wide range of potentially harmful food contaminants and additives. The Raman spectrum for the fungicide thiram is shown in Figure 4.

The sample was prepared by drop casting a solution containing 1×10^{-3} M thiram in acetone to the gold substrate. This toxic fungicide is used to prevent crop damage before and after crop harvest. The toxicity of this fungicide is high enough that it requires protective clothing for handling. As shown in Figure 4, gold SERS substrates and ROS sampling has sufficient sensitivity to detect relatively low levels of this toxic fungicide.

Chloramphenicol is a broad-spectrum antibiotic used in aquaculture. It has been banned for food use and is tightly regulated to avoid toxicity and the potential for the creation of antibiotic-resistant bacteria. As shown in Figure 5, SERS with a gold substrate and ROS sampling enables detection of 1×10^{-3} M concentrations in ethanol of this banned food contaminant.

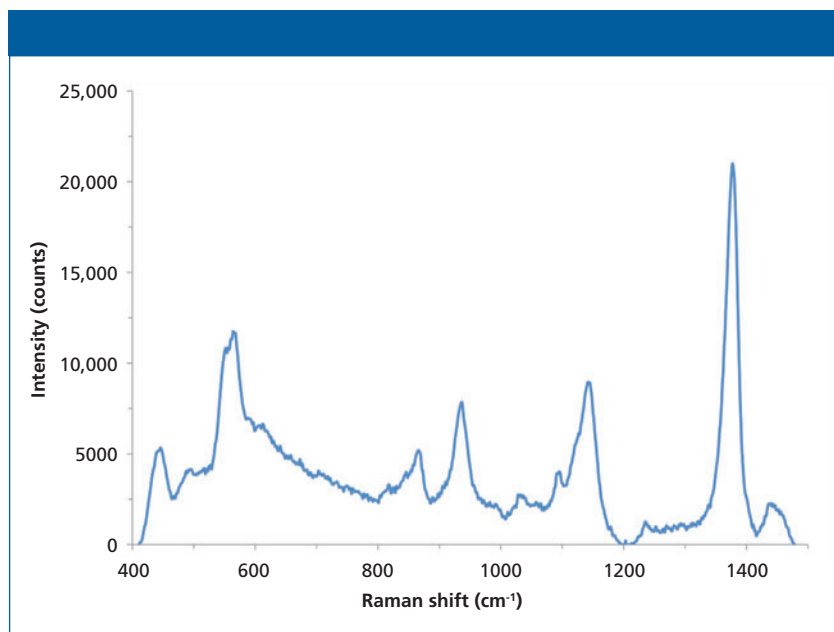


Figure 4: The fungicide thiram on gold SERS: Raman spectrum for 1×10^{-3} M thiram in acetone measured using ROS sampling.

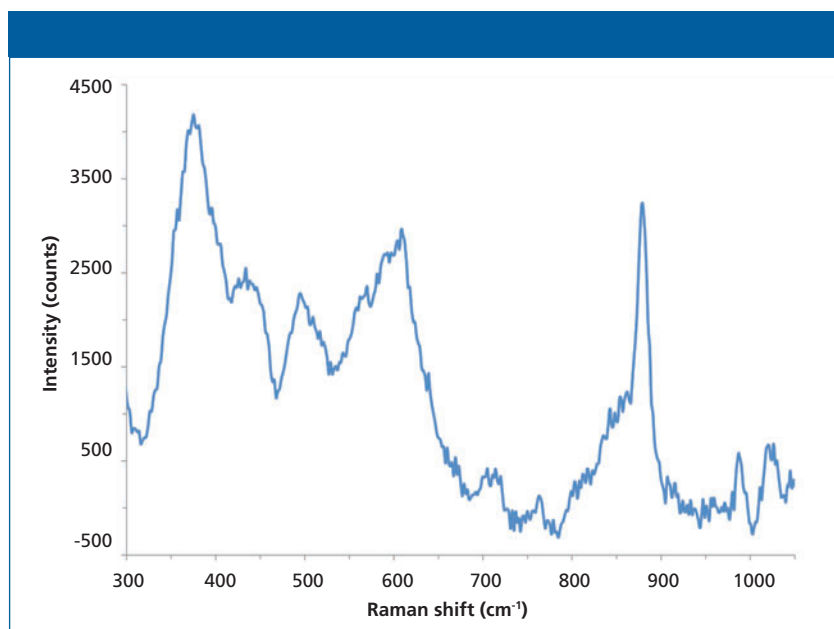


Figure 5: The antibiotic chloramphenicol on gold SERS: Raman spectrum for 1×10^{-3} M chloramphenicol in ethanol measured using ROS sampling.

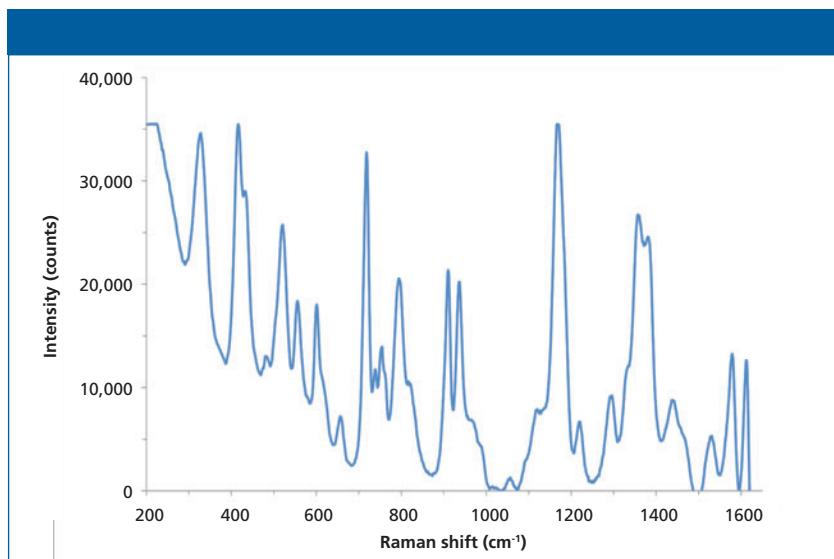


Figure 6: The fungicide crystal violet on gold SERS: Raman spectrum for 1×10^{-4} M crystal violet in ethanol measured using ROS sampling.

In Figures 6 and 7, Raman spectra for the fungicides crystal violet and malachite green are shown. These fungicides are also banned for use in aquaculture because of their toxicity. These antifungal agents are low cost and very effective against fungal and parasite infections in fish, but they are not approved for use in aquaculture because of their potential for mutagenic impact on humans. A comparison of these spectra demonstrates not only the sensitivity of the technique, but also the specificity of Raman analysis. Each fungicide has a distinct spectral fingerprint allowing for discrimination and identification. As shown in Figures 6 and 7, both fungicides are easily detected at 1×10^{-4} M concentrations in ethanol with SERS using gold substrates and ROS sampling.

Conclusion

Food safety is a global concern. Outbreaks and even death have driven the

search for improved technologies to detect very low levels of food contaminants. The tremendous signal enhancement associated with SERS, combined with ROS sampling of highly stable gold substrates, make SERS a good candidate for the detection of trace levels of food additives and contaminants. With recent advances in handheld Raman instrumentation including the availability of handheld devices with ROS sampling, SERS is a viable option for the fast, low cost, and sensitive detection of these dangerous compounds outside the laboratory setting.

References

- (1) K.R. Matthews, in *Practical Food Safety: Contemporary Issues and Future Directions*, R. Bhat and V. Gomez-Lopez, Eds. (John Wiley and Sons, Hoboken, New Jersey, 2014), pp. 1–9.
- (2) D.J. Gardiner, in *Practical Raman Spectroscopy*, D.J. Gardiner and P. R. Graves,

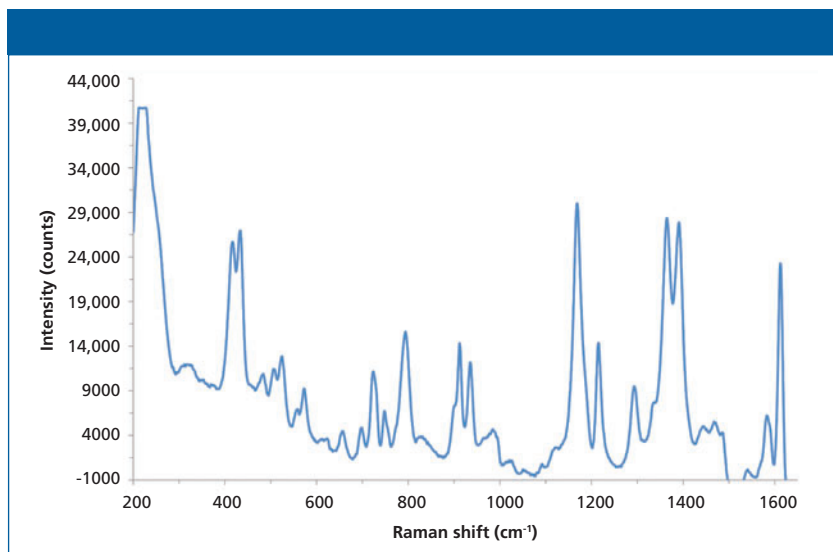


Figure 7: The fungicide malachite green on gold SERS: Raman spectrum for 1×10^{-4} M malachite green in ethanol measured using ROS sampling.

- Eds. (Springer-Verlag, Berlin, Germany 1989), pp. 1–12.
- (3) D.L. Jeanmarie and R.P. Van Duyne, *J. Electroanal. Chem.* **84**, 1–20 (1977).
 - (4) M. Fleischmann, P.J. Hendra, and A.J. McQuillan, *Chem. Phys. Lett.* **26**(2), 163–166 (1974).
 - (5) R.A. Alvarez-Puebla, D.S. Dos Santos Jr, and R.F. Aroca, *Analyst* **129**, 1251–1256 (2004).
 - (6) W.E. Doering and S.M. Nie, *J. Phys. Chem. B* **106**, 311–317 (2002).
 - (7) K. Kneipp and H. Kneipp, *Appl. Spectrosc.* **60**(12), 322A–334A (2006).
 - (8) A.P. Craig, A.S. Franca, and J. Irudayaraj, *Ann. Rev. Food Sci. Technol.* **4**, 369–380 (2013).
 - (9) J. Zheng and L. He, *Comp. Rev. Food Sci. Food Safety* **13**, 317–329 (2014).
 - (10) J.A. Creighton, C.G. Blatchford, and M.G. Albrecht, *J. Chem. Soc. Faraday Trans.* **75**, 790–798 (1979).
 - (11) D.S. Wang, H. Chew, and M. Kerker, *Appl. Opt.* **19**, 2256–2257 (1980).
 - (12) N.L. Rosi and C.A. Mirkin, *Chem. Rev.* **105**, 1547–1562 (2005).
 - (13) M.D. McMahon, R. Lopez, H.M. Meyer, III, L.C.R.F. Feldman, and J.R. Haglund, *Appl. Phys. B* **80**, 915–921 (2005).
 - (14) P. Gao and M.J. Weaver, *J. Phys. Chem.* **89**, 5040–5046 (1985).
 - (15) P. Gao, D. Gosztola, L.W.H. Leung, and M.J. Weaver, *J. Electroanal. Chem.* **233**, 211–222 (1987).
- Yvette Mattley, PhD, Maja Sourdain, Derek Guenther, Cleo Harvey, and Adrian Guckian, PhD,** are with Ocean Optics in Dunedin, Florida. Direct correspondence to: Yvette.Mattley@OceanOptics.com ■

For more information on this topic,
please visit our homepage at:
www.spectroscopyonline.com

REVOLUTIONIZE YOUR MATERIAL IDENTIFICATION

Progeny™

The new generation in
handheld Raman analysis
that streamlines your
material ID workflow.



Accurately analyze your materials
through packaging

Minimize the learning curve with a
smartphone-inspired interface

Increase confidence in your material
ID with unparalleled sensitivity

Measure a wide range of materials
with interference-free data

Expand your data transfer flexibility,
LIMS, wireless, and docking station

IT LOOKS DIFFERENT BECAUSE IT IS DIFFERENT



Rigaku
Rigaku Raman Technologies

Toll Free: +1 855.785.1064

Direct: +1 781.328.1024

www.rigakuprogeny.com

The Use of Portable and Handheld Raman Spectroscopy for Forensic Investigations

The Raman technique is gaining widespread acceptance as an investigative tool for forensic applications. This article focuses on the use of portable and handheld Raman spectroscopy in the field of forensic science and illustrates it with real-world examples.

Katherine Bakeev and Robert Thomas

The benefits of Raman spectroscopy are well recognized for the molecular identification of unknown molecular compounds and as a result the technique is being used routinely in applications areas such as pharmaceutical manufacturing (1), raw material verification (2), detection of counterfeit drugs (3), medical diagnostics (4), characterization of polymers (5), and the quality control of food products (6). However, more recently the technique is gaining widespread acceptance as an investigative tool in the areas of forensic science and homeland security (7,8). On-board spectral libraries and intelligent decision-making software make Raman spectroscopy ideally suited to help law enforcement agencies better understand the source and nature of illicit materials. Today's Raman instrumentation is faster, more rugged, and less expensive, and the advances in component miniaturization have led to the design of portable devices with extremely high performance that can be taken out and used for field-based investigations. Therefore, this study focuses on the use of handheld

Raman spectroscopy for the characterization and identification of samples encountered in various application areas related to forensic science.

The Role of Law Enforcement

Law enforcement agencies responsible for reducing the level of serious crime are being faced with more challenges than ever before. For example, new designer drugs are appearing on street corners around the world almost every day. Additionally, terrorism attacks using various explosive devices are being reported by the media around the globe on a regular basis. Also, a topic of international importance is the increase in production of counterfeit cancer, malaria, prescription, and over-the-counter (OTC) drugs, particularly in parts of the world that do not have the skill and expertise to detect them (9). As a result, there is clearly a need to investigate these events in a speedy and timely manner.

This fact is supported by investigations into the illegal use of both social and performance-enhancing drugs, where an identification needs to be made on the type and source of the ma-

High Performance Lasers by Cobolt.



Cobolt Pulsed Lasers



- Q-switched lasers
- 1064 nm, 532 nm & 355 nm
- Tunable Mid-IR lasers
- 2 – 5 μm , tunable 50 nm

Cobolt CW Lasers



- DPSS and diode lasers
- 355 – 1064 nm
- Extreme spectral purity
- Robust single longitudinal mode performance

Your first choice of laser for advanced spectroscopy applications: Raman, PAS, LIBS and more!

Built with **HTCure™** technology which has enabled Cobolt to supply ultra-robust SLM DPSS lasers with proven reliability for over a decade.

terial used as quickly as possible. Traditionally, test kits are used to obtain a positive indication of a particular drug for presumptive evidence purposes. Unfortunately, for some of the newer, more exotic, and designer drugs of abuse, specific test kits may not be available. Since limited testing can be carried out in the field, seized samples are subsequently sent to a state or federal laboratory for confirmatory analysis. Overburdened laboratories may require weeks or even months before test results reach the prosecutor's hands and, as a result, the pressure placed on analytical chemists to process samples as quickly as possible can be quite significant.

Forensic laboratories that provide evidence for the positive identification of these kinds of samples frequently use gas chromatography–mass spectrometry (GC–MS), which is considered the gold standard for the analysis of volatile organic compounds. However, even though GC–MS provides definitive results, it is a costly, destructive, laboratory-based technique that is extremely time-consuming and contributes to the backlog of samples, subsequently delaying the reporting of results back to law enforcement agencies waiting to prosecute cases.

For that reason, state-of-the-art analytical techniques being used for rapid screening and confirmatory identification are now being miniaturized and making their way into field instrumentation. The transition from laboratory-based to field-based analyzers allows law enforcement agencies to conduct reliable measurements at the point of use, lessening the burden on crime laboratories, reducing their sample backlog, and accelerating the prosecution process. One of the most

exciting analytical techniques that is moving analysis away from the laboratory and into the field is portable Raman spectroscopy. Before we take a look at how this new technique is revolutionizing the forensic analysis landscape, let's take a brief look at its fundamental principles of operation.

Principles of Raman Spectroscopy

Similar to infrared (IR) absorption techniques, Raman spectroscopy measures vibrational, rotational, and other low-frequency modes of a molecule. Whereas IR spectroscopy is based on focusing a broad range of IR wavelengths of light on to the sample and measuring which ones are absorbed, a Raman spectrum is obtained by directing a single wavelength of light and collecting the resulting scattered light. The frequencies of the scattered light depend on the bond strength of the molecules, the mass of the bound atoms, and other factors such as intermolecular interactions. The pattern of vibrational and rotational frequencies from a molecule is highly characteristic of a given molecular species or the structural arrangement of those molecules and, as a result, can be used for the positive identification of that species or compound (10). Because of variations in Raman band intensities and overlapping bands, robust library searching algorithms are needed for reliable identification of samples. Unfortunately, with many sample types, baseline changes caused by fluorescence, scattering effects, and changes in the signal intensity with different power settings can interfere with the Raman measurements. For this reason it is very important that any portable or handheld Raman spectrometer is designed with an understanding that

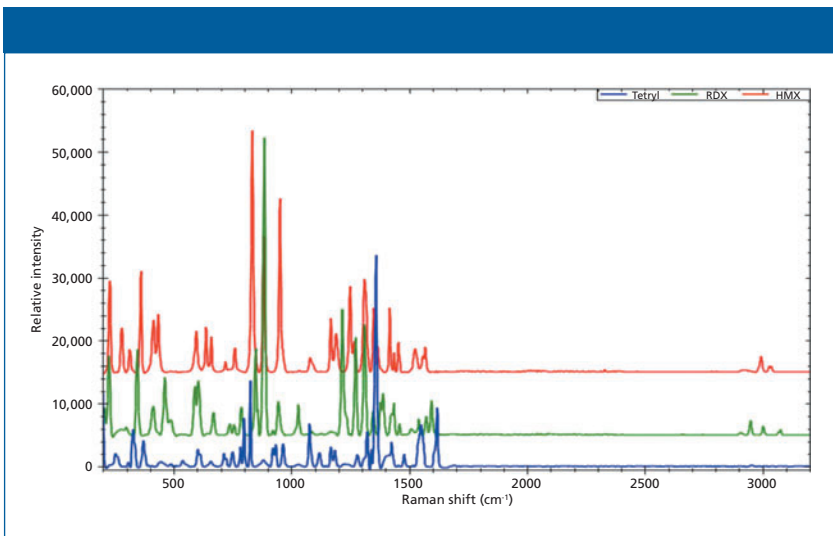


Figure 1: Raman spectra for two nitroamine high explosives (HMX and RDX) in red and green, respectively and 2,4,6-trinitrophenylmethylnitroamine (tetryl) in blue.

these kinds of potential interferences need to be addressed to handle real-world applications.

Instrumentation

This study examines the use of a handheld Raman spectrometer (TacticID, B&W Tek) to carry out the real-world testing of a group of forensic and homeland security-related samples. The fundamental principles of the device have been described in the open literature, but it is basically a field-ready, spectral analysis instrument specifically designed to enable the forensic analysis of unknown chemicals and narcotics. It is a compact spectrometer and integrated computing system weighing approximately 2 lb, and it allows for the confirmation of a sample in less than 30 s.

The system includes a 785-nm, 300-mW laser excitation source with a crossed Czerny-Turner spectrograph and a charge-coupled device (CCD)

array detector. The system provides a stable signal with low background noise, which is very important when testing materials of a similar molecular structure such as narcotics, pharmaceuticals, or hazardous and explosive mixtures because of the potential for other components in the sample to increase the background noise and elevate the baseline through fluorescence or other photon scattering effects.

The system can be customized for specific forensic applications, but the standard configuration contains a library of spectral information generated from more than 4500 chemicals, toxic or hazardous materials, explosives, precursors, narcotics, pharmaceutical drugs, and cutting agents. For example, the hazardous or explosive materials in the spectral library include polynitro aromatics such as trinitrotoluene (TNT) and trinitrobenzene (TNB); nitrate esters or nitroamines such as RDX, Semtex, and nitroglyc-

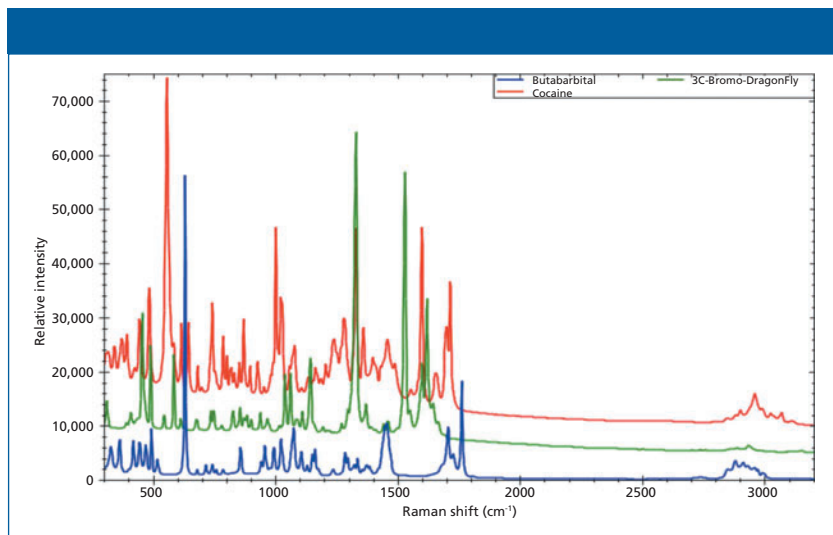


Figure 2: Raman spectra of three narcotics: a barbiturate (butabarbital) in red, a psychedelic drug (3-C bromo-dragonfly) in blue, and cocaine in green.

erin; and a number of different inorganic nitrates and chlorates. Examples of Raman spectra of three explosives in the database are displayed in Figure 1, which shows two nitroamines (HMX and RDX) in red and green, respectively, and 2,4,6-trinitrophenylmethyl-nitroamine (tetryl) in blue. The spectra have been offset for clarity purposes.

A system specifically designed for pharmaceutical and narcotics identification is available (TacticID-N, B&W Tek) that contains nearly 1000 spectra, including Class A drugs such as ecstasy, cocaine, methadone, and phencyclidine (PCP); Class B drugs like amphetamines and methylphenidate (Ritalin); and Class C drugs such as tranquilizers together with many OTC and prescription painkillers. Examples of Raman spectra of three narcotics are demonstrated in Figure 2, which shows a barbiturate (butabarbital) in red, a psychedelic drug (3-C bromo-dragonfly) in blue,

and cocaine in green. Once again, all spectra are offset for clarity purposes.

Real-World Testing Procedures

The testing procedure for real-world samples involves either using the supplied spectral libraries for reference and identification purposes or calibrating the device using pure forms of each of the chemical or drug compounds to develop user-defined libraries to test all the unknown materials under investigation. A proprietary software algorithm is included in the handheld unit in which the Raman spectrum is compared and matched with that in the library to generate a numerical hit quality index (HQI) value from which the result is determined. Analyzing samples in this way with spectral libraries ensures the identification of samples based on the Raman signature that can be related to the unique characteristics of the chemical materials, and provides a reliable testing procedure.

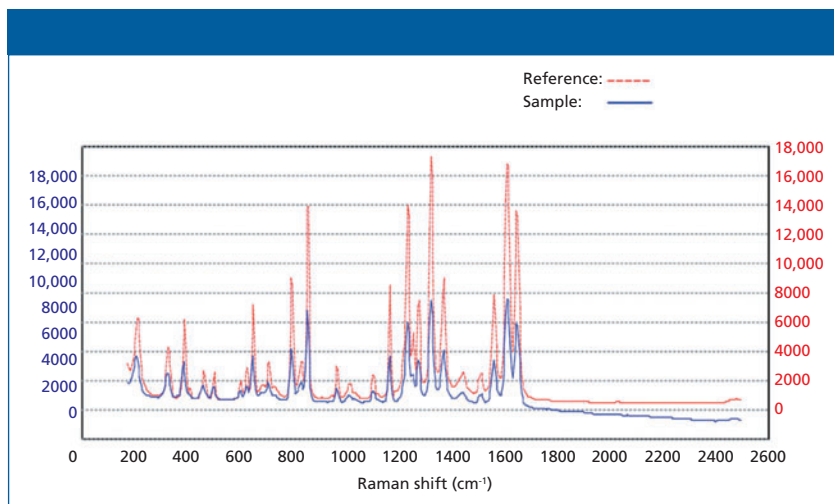


Figure 3: Raman spectra of pure acetaminophen in red (reference) and Tylenol, an OTC pain medication containing acetaminophen, as the active ingredient in blue (sample), indicating a positive match.

ture for unskilled operators required for the unambiguous identification of unknown materials. In routine use, the total scan time and decision making process takes approximately 30 s to make an assessment of a material and whether a match has been found. This is exemplified in Figure 3, which shows a Raman spectrum of pure acetaminophen in red (reference) and Tylenol (McNeil-PPC, Inc.), an OTC pain medication containing acetaminophen, as the active ingredient in blue (sample). The spectra have been offset slightly for clarity purposes, but it can be clearly seen that both spectra are almost identical, indicating a positive match.

Figure 4 shows a positive match for a sample of cocaine (blue) compared to a reference standard (red). This spectrum was actually supplied by a major metropolitan law enforcement agency in the United States, whose police officers were using it for the identification of street drugs.

Figure 5 shows the identification of the explosive TNT. The Raman spectrum of reference TNT standard is shown in red, and the unknown sample is shown in blue. Once again it can be seen that both spectra are almost identical, indicating a positive match.

If a positive identification cannot be found because of a weak Raman signal or high fluorescence, or there is just no match in the spectral library, “no match” will be displayed on the screen. Figure 6 shows a Raman spectrum for which no reference match was found in the library. When this happens, the user can submit the spectrum for further analysis and after positive identification is made, the library can be updated.

Final Thoughts

There will always be a need for law-enforcement and homeland security agencies to characterize and identify narcotics and chemicals that have been used for illegal purposes.

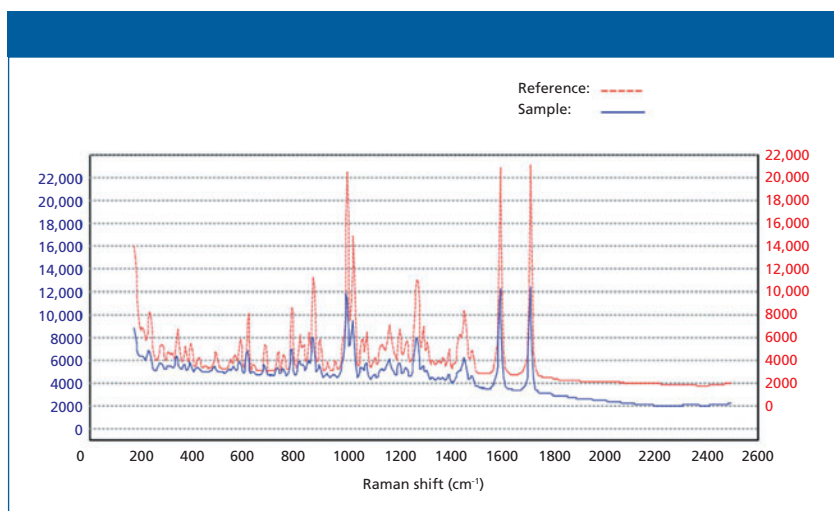


Figure 4: Raman spectra of cocaine showing a positive match for a street sample (blue) compared to a reference spectra (red).

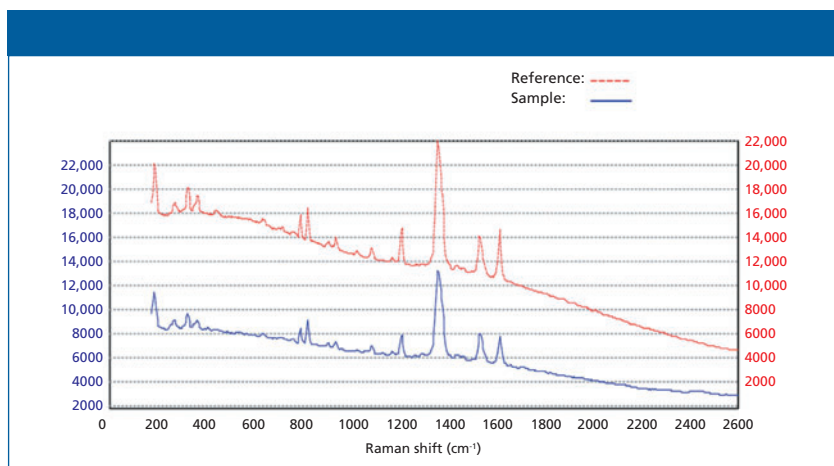


Figure 5: Raman spectrum of pure TNT in red (reference) and an explosive containing TNT in blue (sample), indicating a positive match and identification.

Whether they are drugs of abuse, performance-enhancing drugs, counterfeit prescriptions, OTC medications, or hazardous and explosive materials used in acts of terrorism, the source, nature, and classification of these materials is critical to unravel the crimes committed behind their use. Hand-

held Raman spectroscopy is proving that it is ideally suited for this task.

References

- (1) E. Lozano Diz, *Pharmaceutical Manufacturing*, January 2013. Available at: <http://www.pharmamanufacturing.com/articles/2013/006/?page=full>.

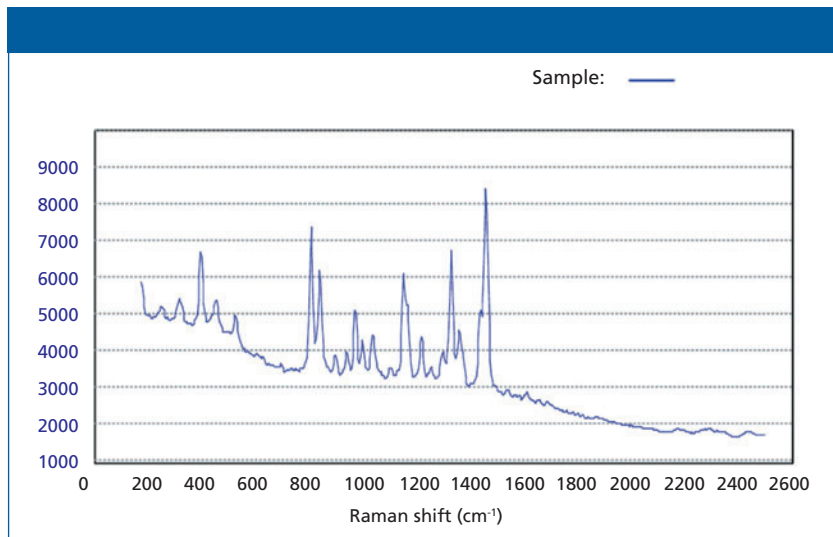


Figure 6: Raman spectrum of an unknown sample where no reference match was found in the library.

- (2) D. Yang and R. Thomas, *Am. Pharm. Rev.* (2012). Available at: <http://www.americanpharmaceuticalreview.com/Featured-Articles/126738-The-Benefits-of-a-High-Performance-Handheld-Raman-Spectrometer-for-the-Rapid-Identification-of-Pharmaceutical-Raw-Materials/>.
- (3) R. Kalyanaraman, M. Ribick, and G. Dobler, *Eur. Pharm. Rev.*, "Non-destructive Materials Identification Supplement," **17**(5), 11–15 (2012).
- (4) R. Thomas, K. Bakeev, M. Claybourn, and R. Chimenti, *Spectroscopy* **28**(9), 36–43 (2013).
- (5) *Vibrational Spectroscopy of Polymers: Principles and Practice*, N.J. Everall, J. Chalmers, and P.R. Griffiths, Eds. (John Wiley and Sons, Chichester, UK, 2007).
- (6) B. Diehl, C.S. Chen, B. Grout, J. Hernandez, S. O'Neill, C. McSweeney, J.M. Alvarado, and M. Smith, *Eur. Pharm. Rev.*, "Non-destructive Materials Identification Supplement," **17**(5), 3–8 (2012).
- (7) E.L. Izaki, *Forensic Sci. Int.* **202**, 1–8 (2010).
- (8) J.F. Kelly, T.A. Blake, B.E. Bernacki, and T.J. Johnson, *Int. J. Spectrosc.* **2012**, Article ID 938407 (2012).
- (9) "Arrest in Cancer Drug Sales in Turkey," *Wall Street Journal*, February 14, 2014. Available at: <http://online.wsj.com/news/articles/SB10001424052702304703804579383271726960510>.
- (10) *Handbook of Raman Spectroscopy*, I.R. Lewis and H.G.M. Edwards, Eds. (Practical Spectroscopy Series 28, Marcel Dekker, New York, 2001).

Katherine Bakeev, PhD, is the director of analytical services and support at B&W Tek in Newark, Delaware. **Robert Thomas** is the principal consultant at Scientific Solutions Inc., in Gaithersburg, Maryland. Direct correspondence to: katherineb@bwtek.com ■

For more information on this topic, please visit our homepage at: www.spectroscopyonline.com

Key Elements of Confocal Raman Microscopy for High-Resolution Imaging

The sensitivity of a high-resolution Raman imaging system is crucial to the quality of the acquired information. The spectral and spatial resolutions are among the primary factors that influence the obtainable results. The limits of resolution are defined theoretically by the laws of physics, but are experimentally determined by the instrument parameters. In this article, the theoretical background and the possibilities in practical applications are discussed.

Thomas Dieing, Marius Henrich, and Sonja Breuninger

Confocal Raman microscopes are the instruments of choice for many Raman measurements in a wide variety of applications ranging from geosciences (1–3), biology (4–6), nanocarbon materials (7–9) to pharmaceutical compounds (10,11), just to name a few. This article sheds light on the possibilities and, in part, the origins in terms of spectral and spatial resolution for confocal Raman systems in general.

Spectral Resolution

Any confocal Raman system will have a spectral resolution which is mainly determined by the following parameters:

- the focal length of the spectrometer (the longer the focal length, the higher the spectral resolution)
- the grating (the higher the groove density, the higher the spectral resolution)
- the pixel size on the charge-coupled device (CCD) camera (the smaller the pixels, the higher the spectral resolution)
- the entrance slit or pinhole (the smaller the slit or pinhole the higher the spectral resolution)
- the line shape preservation (equals imaging quality) of the spectrometer.

In some cases, one of the parameters can put limitations on the spectral resolution. If, for example, the projection of the pinhole onto the CCD is already large compared to the pixel size on the CCD camera, then a further reduction of pixel size will not increase the spectral resolution.

Please note that the microscope components such as the objective used for collection of the signal should not influence the spectral resolution if the entrance slit or pinhole is the limiting element. This is preferential with confocal Raman microscopes.

The determination of the spectral resolution is often a point of debate. First, one should clearly differentiate the spectral resolution from the sensitivity of the system to detect shifts of

CBEx

Handheld Raman System

SnRI offers CBEx, a hand-held Raman identification system, featuring very high sensitivity detection and robust search algorithms for fast, confident results. The 11 hour operational time from two AA batteries provides flexibility in the field where rechargeable systems fail. CBEx is your solution to Site Specific Exploration (SSE).



- Large area Orbital Raster Sampling (ORS™)
- Internal calibration
- High-efficiency spectrograph
- Advanced spectral processing
- 11 hour operation (2 AA batteries)
- 3.6" x 2.8" x 1.5" (9.1 x 7.1 x 3.8 cm)

SnRI

The Peak of Spectroscopy

www.wysri.com



Snowy Range
INSTRUMENTS

individual peaks. Relative peak shifts can be detected with a much higher accuracy using fitting algorithms as has been demonstrated with a sensitivity down to 0.02 rel. 1/cm standard deviation of the peak shift of a Si peak (12). The maximum achievable fit accuracy depends heavily on the number of detected photons and the width of the peak that is fitted. This shift analysis is especially relevant for examining stress within a sample, but may not be taken as a measurement for the spectral resolution.

The spectral resolution, which determines how the system can measure (that is, full width at half maximum [FWHM] of a narrow peak or how well overlapping peaks can be differentiated), needs to be addressed separately from the peak shift sensitivity. There are various ways to state the spectral resolution, and some of the most common ones are outlined below.

Pixel Resolution

The *pixel resolution* is the difference in wavenumbers when moving from one pixel on the CCD camera to the next and is independent of factors such as slit width or peak width of the detected peak. This can only be seen as the true resolution limit if the pixel size and not the size of the entrance slit or pinhole is the limiting factor. For example, if the image of the slit or pinhole on the CCD camera is 100 μm in diameter and the pixel size on the CCD camera is 26 μm , then the resolution would be significantly worse than the distance (in wavenumbers) between two pixels. Since wavenumbers are measured in reciprocal space, it also needs to be noted that the pixel resolution will differ depending on the spectral position

where it is determined. The resolution close to the Rayleigh line can, in this way, differ by almost a factor of two from the pixel resolution near 3500 rel. 1/cm in the case of 532-nm excitation.

Two-Pixel Criterion

For this criterion two times the pixel resolution is taken. The logic behind this is that to discriminate two neighboring peaks one needs to have one pixel on one peak, one in the minimum between the peaks, and a third one on the next peak. This criterion is analogous to the Nyquist theorem in signal processing. The same limitations as outlined for the pixel resolution criterion apply in this case.

Full Width at Half Maximum of Atomic Emission Lines

Atomic emission lines are typically much narrower than any Raman line. Their narrow width makes them a good probe to check the resolution. Figure 1 shows an atomic emission line of mercury near 579.07 nm. The *x*-axis is given in units of rel. 1/cm assuming a 532.00-nm excitation laser. The spectrum was recorded using a mercury and argon calibration lamp coupled via a 10- μm core diameter multimode fiber to a UHTS300 spectrograph (WITec GmbH) equipped with both 1800- and 2400 grooves/mm gratings (BLZ at 500 nm) and a Newton electron multiplying charge coupled device (EMCCD) camera with a pixel size of 16 μm . The integration time was 0.1 and 0.24 s, respectively, for the spectra. The FWHM derived through this approach is a good measure of the resolution, but care must be taken to ensure that enough points are available within the curve to ensure a good fit to the curve.

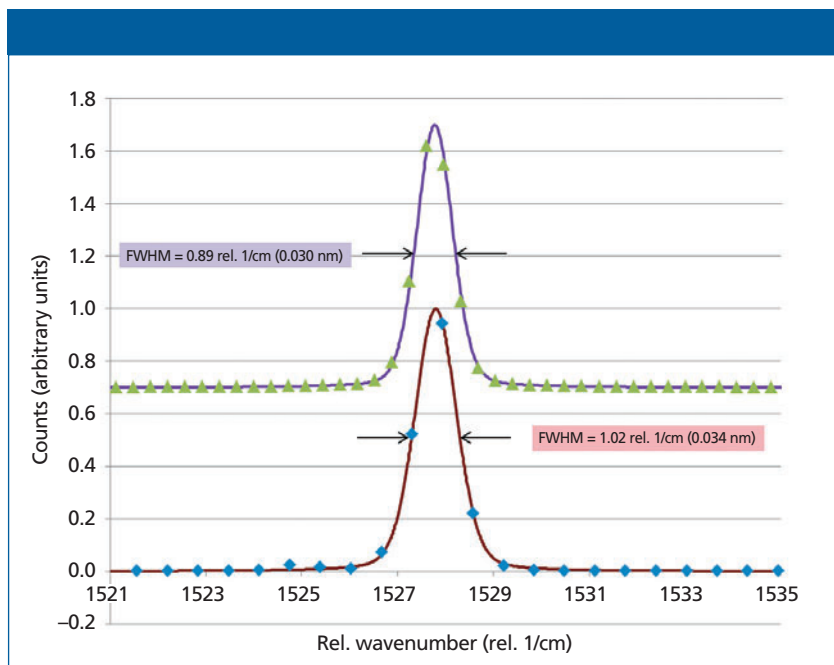


Figure 1: Spectra of the mercury atomic emission line at 579.066 nm plotted as a function of wavenumber assuming a 532.00-nm excitation. The red line is the fitted curve (pseudo voight function) and the blue diamonds are the measured data points for the 1800-grooves/mm grating. The green triangles and the purple curve show the results obtained using the 2400-grooves/mm grating.

Measurement of Peak Resolution on Known Reference Samples

There are a few samples that are established standards to demonstrate spectral resolution. The most prominent is probably CCl_4 . Figure 2 shows two spectra of this substance recorded with different spectral resolutions. It can clearly be seen, that the peaks are nicely separated in the red spectrum whereas the separation is not as clear for the purple spectrum.

Therefore, spectral resolution can be defined in many different ways and, thus, it is advisable to specify exactly how a spectral resolution was or should be determined. Comparing actual measurement results under identical measurement conditions is certainly

one of the best ways to illustrate this. It should also be noted that with few exceptions the natural linewidths of Raman lines are typically larger than 3 rel. 1/cm. Taking the Nyquist criterion into consideration, a resolution in the range of 1 rel. 1/cm should be sufficient for the majority of samples.

Spatial Resolution

When considering the spatial resolution of a confocal Raman microscope one may distinguish between the lateral (x and y) resolution and the depth resolution. However, in either case, it is possible that the limitations arise because of one of the five following points:

- basic physics (that is, diffraction limit)

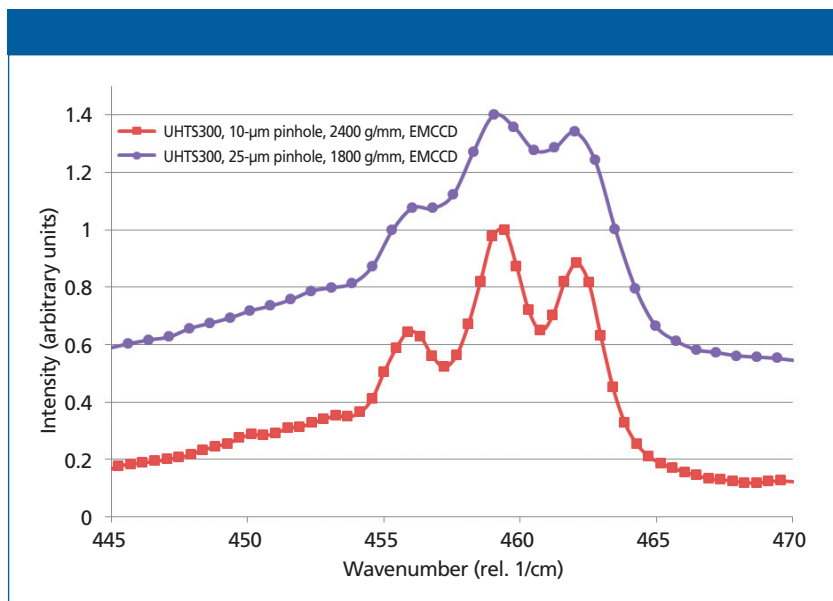


Figure 2: Raman spectrum of CCl_4 with 532-nm excitation at different spectral resolutions.

- limited positioning accuracy of the mechanical components used
- limitations because of the optical components used in the beam path (that is, beam distortion)
- nondiffraction limited sample illumination
- pixel resolution of the image acquired.

In terms of the positioning system, it is important to differentiate the single step accuracy of a stepper motor, the positioning reproducibility, and linearity. The reproducibility and linearity are the key factors for an imaging system since this allows a line by line imaging. If, for example, a straight line is imaged, then this line will only be imaged with the accuracy of the positioning reproducibility even though the step size might be much smaller. Figure 3 illustrates this effect with Figure 3a showing insufficient positioning reproducibility and

Figure 3b showing sufficiently high positioning reproducibility.

The necessary positioning reproducibility should therefore be several factors better than the smallest imaged object, or if the system should allow the best physically possible resolution, several factors (that is, $10\times$) better than the diffraction limit.

Using high-quality components and positioning systems should allow imaging approaching the limits of physics.

Lateral Resolution

Based on the diffraction theory of Ernst Karl Abbe, Lord Rayleigh defined the diffraction limit in 1896. Rayleigh thereby quantified the minimal distance at which two point light sources can be identified. In this case, one of the sources is located at exactly the distance of the first minimum of the Airy function (point spread function) of the other one. This distance (d_{lim}) can be

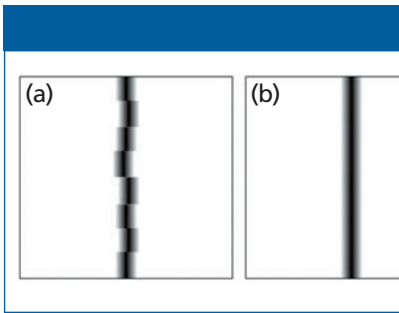


Figure 3: A straight line imaged with (a) insufficient positioning reproducibility and (b) sufficient positioning reproducibility.

expressed as a function of the wavelength emitted (λ) and the numerical aperture (NA) of the objective used as:

$$d_{lim} = 0.61 \frac{\lambda}{NA} \quad [1]$$

The equation $1.22 \lambda/NA$ is often also found in this context, but this describes the distance between the two first minima of the Airy function and not the diffraction limit as described by Lord Rayleigh. Using the definitions of the Airy function the resolution can be easily derived by how much the intensity between the two emitting points has to decrease according to the Rayleigh criterion. Please note that the distance is different for other criteria of diffraction such as the Abbe criterion or the Sparrow criterion.

To derive the resolution of a microscope using either of those criteria it would be necessary to have a variety of very small, well scattering objects (small compared to the size of the Airy disk; for example individual TiO_2 particles) at varying distances. Following high-resolution Raman imaging, one would then have to analyze the signal intensities and based on the detect-

able distances between the spots one would have to derive the resolution.

An easier way to determine the lateral resolution power of a system uses the FWHM of small objects. Based on the Airy function the relation between the FWHM of the light emitted from an object and the diffraction limited distance (d_{lim}) is

$$FWHM \approx 0.85 d_{lim} = 0.51 \frac{\lambda}{NA} \quad [2]$$

Because the measured signal is always a convolution between the object size, the emission characteristics, and the system function, the objects measured in such experiments also have to be small compared to the Airy disk. Mathematically speaking, the object's size should approach a delta function for the convolution. Such small objects naturally have only limited material which scatters and thus one may expect small Raman signals emitted by them. Carbon nanotubes (CNTs) on the contrary show a large Raman signal while being very small in diameter (typically ranging from subnanometer to a few nanometer range) and comparatively long (up to a few micrometers typically). These samples are thus the ideal probes to check the lateral resolution of a confocal Raman microscope. For a 532 nm excitation laser and an objective with an numerical aperture (NA) of 0.9 one should therefore be able to obtain a FWHM across CNTs of about 301 nm.

Figure 4a shows the integrated intensity of the G-band on a sample of CNTs on a Si substrate. The scan range was $1.5 \mu m \times 1.5 \mu m$ with 50×50 points and an integration time of 23 ms per point was used. An alpha300R system (WITec GmbH) was

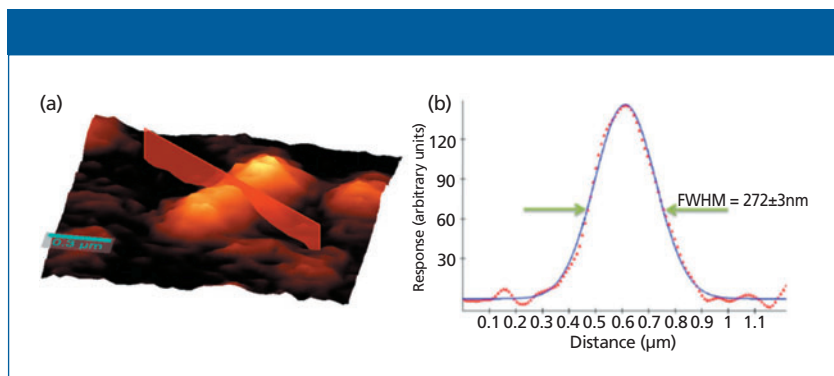


Figure 4: Integrated intensity of the G-band of a carbon nanotube with (a) the cross section position marked in red and (b) the cross-sectional intensity along this line. The lateral resolution of the microscope system can be characterized by the FWHM and is about 272 nm.

used for the measurement in combination with a fiber-coupled, frequency-doubled Nd:YAG laser (532 nm emission), a Zeiss 100× NA 0.9 objective, and a 50-μm multimode fiber acting as the pinhole for confocal microscopy. For this microscope and objective this corresponds to a projected pinhole size of 500 nm in the focal plane. The spectrometer used was a UHTS300 (WITec GmbH) with a 600-grooves/mm grating (BLZ at 500 nm) combined with a back-illuminated CCD camera.

The red line in Figure 4a indicates where the cross section shown in Figure 4b was extracted from. It can clearly be seen that the FWHM is even narrower than the predicted minimum.

The theory of confocal microscopy (for example, see reference 13) shows that the achievable resolution can further be decreased by a maximum of $1/\sqrt{2}$. In confocal Raman microscopy this fact is rarely used to its limit, because it requires a strong reduction of the pinhole diameter, which in turn reduces the throughput.

Depth Resolution

Depth resolution is the best proof of the confocality of a system. The instrument design has a key influence on the achievable resolution, but the pinhole or slit as well as the way the sample is illuminated also play a crucial role for the depth resolution. Therefore, these points are outlined below before the physical limit of the depth resolution is discussed.

Pinhole or Slit

The pinhole plays a crucial role for the depth resolution in confocal microscopy. However, the physical size of the pinhole ($P_{physical}$) cannot easily be compared between different instruments. In image generation using two simple lenses, the focal length of both lenses contributes to the ratio between the object and the image size. This of course also holds true for a microscope. Here, we have the magnification of the objective ($M_{Objective}$), which is calculated for a certain focal length of the tube or telan lens ($f_{Tube, Objective}$). This focal length ranges for commercial microscopes from 164.5 mm for Zeiss

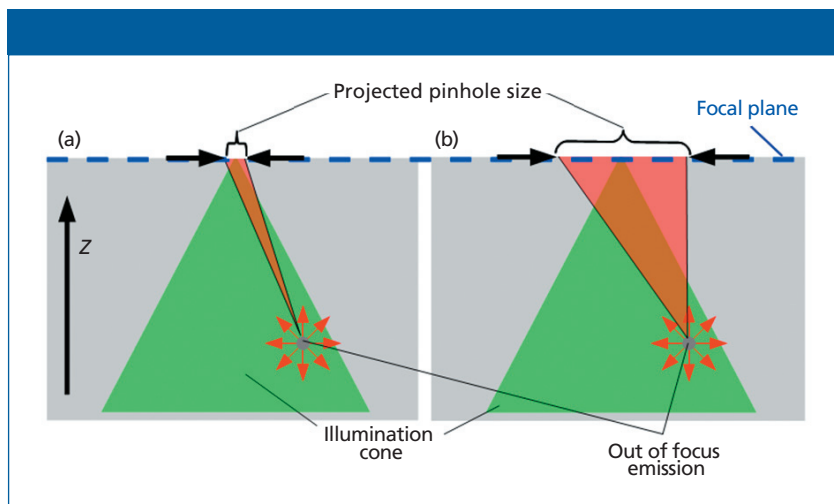


Figure 5: The light collected from an out of focus emitter through the projected pinhole and thus the physical pinhole for the case of (a) a small pinhole and (b) a large pinhole or slit.

objectives up to 200 mm for Leica or Nikon objectives. The magnification printed on the objective is only correct if the objective is designed for the tube focal length of the microscope. To have a comparable value for the pinhole size one should therefore calculate the projected pinhole size (P_{proj}) as follows:

$$P_{proj} = \frac{P_{physical}}{M_{eff}} = \frac{P_{physical}}{M_{Objective} \frac{f_{Tube, Objective}}{f_{Tube, real}}} \quad [3]$$

The same calculation also applies if a slit is used as a pinhole. For the following considerations, we will use the projected pinhole instead of the physical pinhole size.

The influence of the projected pinhole size is illustrated in Figure 5. Here, a point illumination of a small area with an objective with a relatively high NA value is assumed. The collection diameter of the objective is assumed to be larger than the area

shown and, thus, this is assumed not to be the limiting factor here.

If the sample is transparent enough, the light will propagate further through the sample beyond the focal plane as shown by the illumination cone in Figure 5. This light can excite out-of-focus molecules, which can then emit light (Rayleigh, fluorescence, Raman, and so on) in turn. This emission is isotropic, so part of the light will find its way through the position of the projected pinhole in the focal plane and, thus, also through the physical pinhole. When comparing Figures 5a and 5b, it is apparent that a large pinhole allows a much higher amount of out of focus light to be detected. Therefore, a larger pinhole as well as a slit can never achieve the same suppression of out of focus light compared to a small pinhole.

Sample Illumination

In the last section it was shown that part of the emission from out-of-focus

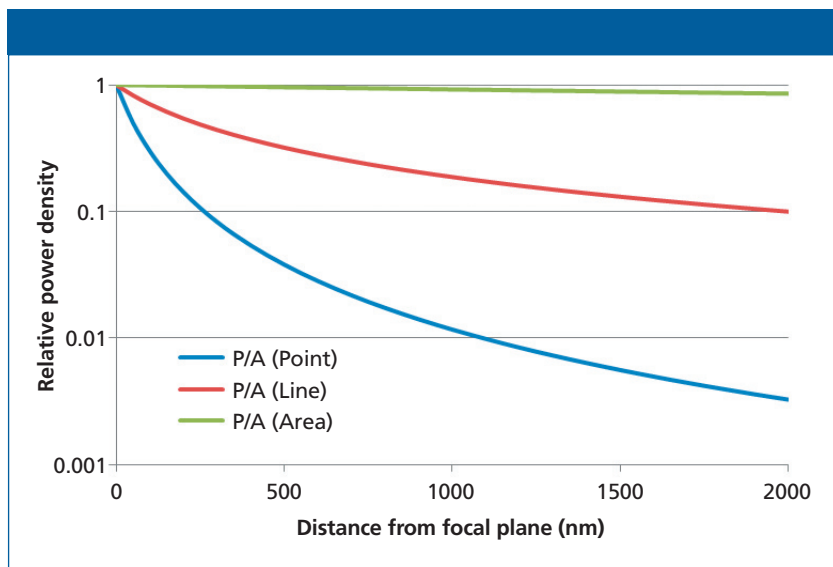


Figure 6: Relative laser power density as a function of distance from the focal plane.

material will always pass through the pinhole and that the contribution of this emission to the detected signal is highly dependent on the pinhole size. The intensity of the excitation light at such an out-of-focus position is, in addition, directly proportional to the emitted light. This intensity is decreasing with an increasing distance of the point from the focal plane. The strength of this decrease, however, is heavily dependent on the way the sample is illuminated and can best be compared by taking the power density (power or area) into consideration. Given a fixed illumination power, one can simply take the increase in the illuminated area as a function of depth into consideration. The numerical aperture of the objective is essential in this consideration. The higher the numerical aperture, the faster the increase of the area as a function of depth and, thus, the faster the decrease of the power density as

a function of depth. In addition to the numerical aperture, the way the sample is illuminated plays a key role. Global illumination shows the smallest decrease as a function of depth. Line illumination shows a faster decrease and point illumination gives the fastest decrease of the laser power density as a function of depth (see Figure 6). For the example shown, a point focus of $0.5 \mu\text{m}$ diameter, a line focus of $1 \mu\text{m} \times 100 \mu\text{m}$, and a global illumination of $100 \mu\text{m}$ diameter was used. The NA value used for the calculations was 0.9. For this approximation, a truncated cone was used as the geometry of the point and global illumination and a truncated pyramid were used for the line illumination.

Real-world samples have additional absorption of the laser power as a function of depth, but this would affect all three curves similarly.

Thus, when comparing point illumination with a confocal pinhole

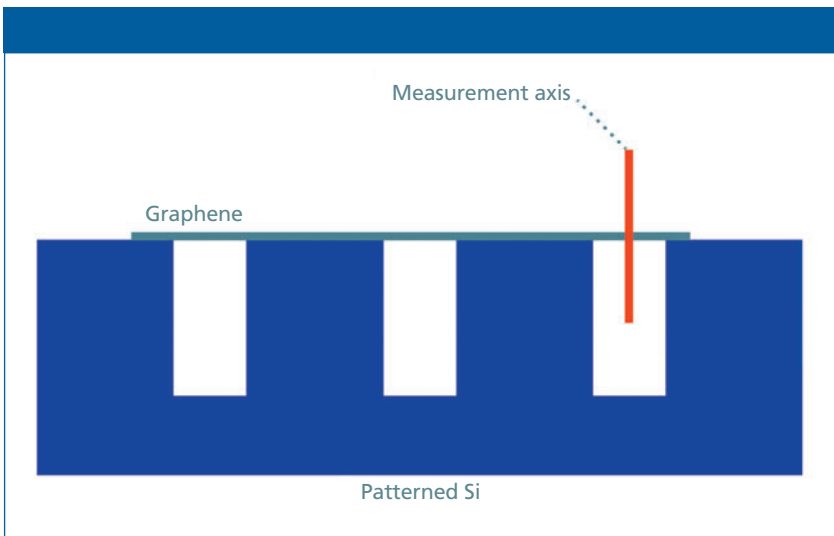


Figure 7: Graphene is suspended over holes in Si to determine the depth resolution. The red line displays the measuring position.

and line illumination with a slit, it is apparent that more light of the out-of-focus emitters passes through the pinhole (see Figure 5) and, in addition, the power density in these out of focus planes is significantly higher (in the example shown in Figure 6 it is a factor of ~ 16 at a 1000-nm depth). The depth resolution achievable with line or global illumination cannot achieve the same values as point illumination. All of the following considerations are therefore calculated and measured for a point illumination and a circular pinhole.

Theory and Measurement of Depth Resolution

For the prediction of the possible depth resolution in confocal Raman microscopy one commonly uses the theory applicable for small numerical apertures (for example see reference 13). This theory predicts a minimal achievable FWHM in the z -direction (at minimal

pinhole diameter) of about 940 nm for a 532-nm laser and a 0.9-NA objective.

To probe this depth resolution one can perform a depth scan on silicon (Si), which shows a very small penetration depth for 532-nm excitation, is available in virtually every laboratory, and has a strong Raman signal. Following the discussion outlined for the lateral resolution, however, a very thin sample would be ideal. Graphene or ultrathin graphite (that is, 5–10 atomic layers) suspended over holes in Si is an ideal sample to illustrate this (see Figure 7 for a schematic of the sample). Similar to the CNTs for the lateral resolution, graphene has a very strong Raman signal and can act as an approximation for a delta function for the convolution of the sample geometry with the system function.

Figure 8a shows a depth profile of the integrated intensity of the first order Si peak (red) and the integrated intensity of the peak near 1600 *rel.* 1/cm recorded on suspended ultrathin

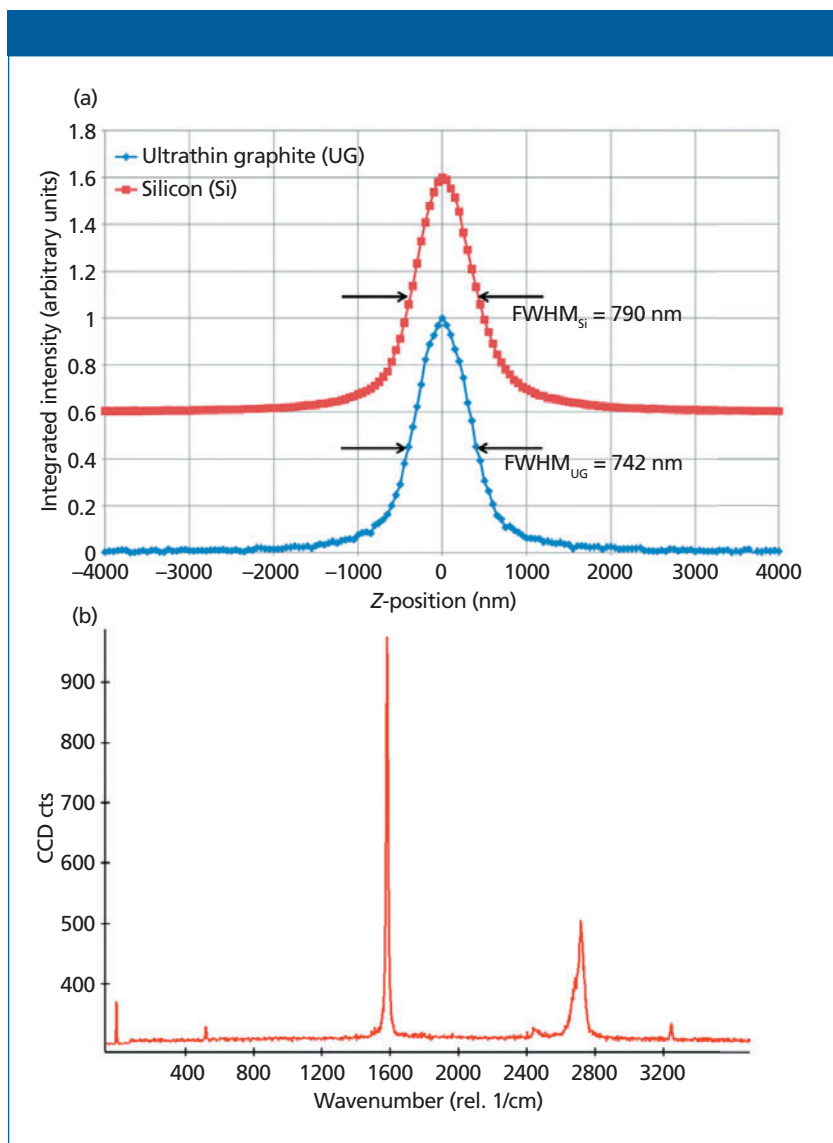


Figure 8: (a) Depth profile on suspended ultrathin graphite and Si. (b) A single spectrum on suspended ultrathin graphite (integration time 2 s).

graphite. The system used was an alpha300R microscope (WITec GmbH) with a $100\times$ NA 0.9 Zeiss objective, a $10\text{-}\mu\text{m}$ pinhole (100 nm projected pinhole diameter), and a UHTS300 spectrometer (WITec GmbH). The

integration time per point was 2 s and the step width was 50 nm. The z -position was set by an interferometrically calibrated piezoelectric positioning table. The depth profiles in Figure 8a are offset for clarity. Figure 8b shows

the spectrum of the ultrathin graphite in focus with a 2-s integration time.

A close comparison of the depth profile of Si with the one collected from ultrathin graphite shows that the rising part of the curve (negative z -position values; above the sample surface) are virtually identical. The falling half (positive z -position values; below the sample surface) shows a broadening for the Si curve. This broadening is because of the penetration of the laser into Si. This penetration depth is small for a green laser and Si, but would be considerably more for a near-IR laser and, thus, the curve of Si would be further distorted on the falling half. For excitation using a green laser source this comparison shows, however, that the commonly available Si can be used as a very good probe to obtain information on the depth resolution of a system.

Comparing these results to the theory for low numerical apertures illustrates that it cannot be valid for high numerical apertures. Converting this theory to match the high numerical aperture case is not trivial, but an approximation can be given following the work by Mack (14). Based on this, the ratio between the low numerical aperture and the high numerical aperture results can be calculated as

$$\frac{\text{low NA result}}{\text{high NA result}} = \frac{4 \sin^2\left(\frac{\Theta}{2}\right)}{\sin^2(\Theta)} \quad [4]$$

where Θ is half of the opening angle of the objective. For an NA value of 0.9 this results in a correction factor of 1.38. Thus, the best depth resolution achievable according to this approximation should be about 682 nm.

The work by Wilhelm and colleagues (15) for confocal laser scan-

ning microscopy can also be followed for this purpose. From this we find an axial optical resolution dependent on the projected pinhole size. For projected pinhole sizes larger than one "Airy unit" ($1.22 \cdot \lambda / \text{NA}$) the following equation applies:

$$\text{FWHM}_{\text{axial}} = \sqrt{\left(\frac{0.88 \cdot \lambda_{\text{em}}}{(n - \sqrt{n^2 - \text{NA}^2})}\right)^2 + \left(\frac{\sqrt{2} \cdot n \cdot P_{\text{proj}}}{\text{NA}}\right)^2} \quad [5]$$

where λ_{em} refers to the emitted wavelength. Using the experimental parameters shown above with $\lambda_{\text{em}} = 580.7$ nm, this results in an axial FWHM of 920 nm. It should be noted however, that the projected pinhole size is significantly smaller than the Airy unit in the presented data. For this case, the work by Wilhelm (15) suggests a different equation as follows:

$$\text{FWHM}_{\text{axial}} = \frac{0.64 \cdot \bar{\lambda}}{(n - \sqrt{n^2 - \text{NA}^2})} \quad \text{with } \bar{\lambda} = \sqrt{2} \frac{\lambda_{\text{em}} \cdot \lambda_{\text{exc}}}{\sqrt{\lambda_{\text{exc}}^2 + \lambda_{\text{em}}^2}} \quad [6]$$

With this, the calculated result is about 630 nm FWHM.

These theories do not result in the same axial resolution, which clearly indicates that there are some inconsistencies in the calculations (that is, between equations 4 and 6). It can however, clearly be seen both from the theories as well as experimentally, that FWHMs well below 1 μm are possible and can be expected from confocal Raman microscopes.

Summary

Confocal Raman microscopes allow the measurement of nanometer-size objects and, using such objects, the

spatial resolution of the systems can be easily determined. The experimental results that are routinely achieved are very close to the theoretical predictions. The spectral resolution needs to be clearly defined and standard samples or light sources are best used to determine this. A reliable comparison should ideally duplicate all relevant parameters and, for example, require all resolution measurements to be performed using the same projected pinhole size.

References

- (1) P. Jenniskens, M.H. Shaddad, D. Numan, S. Elsir, A.M. Kudoda, M.E. Zolensky, L. Le, G.A. Robinson, J.M. Friedrich, D. Rumble, A. Steele, S.R. Chesley, A. Fitzsimmons, S. Duddy, H.H. Hsieh, G. Ramsay, P.G. Brown, W.N. Edwards, E. Tagliaferri, M.B. Boslough, R.E. Spalding, R. Dantowitz, M. Kozubal, P. Pravec, J. Borovicka, Z. Charvat, J. Vaubaillon, J. Kuiper, J. Albers, J.L. Bishop, R.L. Mancinelli, S.A. Sandford, S.N. Milan, M. Nuevo, and S.P. Worden, *Nature* **458**, 485–488 (2009).
- (2) A. Rotundi, G.A. Baratta, J. Borg, J.R. Brucato, H. Busemann, L. Colangeli, L. D'Hendecourt, Z. Djouadi, G. Ferrini, I.A. Franchi, M. Fries, F. Grossemy, L.P. Keller, V. Mennella, K. Nakamura, L.R. Nittler, M.E. Palumbo, S.A. Sandford, A. Steele, and B. Wopenka, *Meteorit. Planet. Sci.* **43**, 367–397 (2008).
- (3) C. Heim, J. Lausmaa, P. Sjövall, J. Toporski, T. Dieing, K. Simon, B.T. Hansen, A. Kronz, G. Arp, J. Reitner, and V. Thiel, *Geobiology* **10**, 280–297 (2012).
- (4) S. Hild, F. Neues, N. Znidarsic, J. Strus, M. Epple, O. Marti, and A. Ziegler, *J. Struct. Biol.* **168**, 426–436 (2009).
- (5) N. Gierlinger and M. Schwanninger, *Spectroscopy* **21**, 69–89 (2007).
- (6) A. Hermelink, A. Brauer, P. Lasch, and D. Naumann, *Analyst* **134**, 1149–1153 (2009).
- (7) Y.N. Xu, D. Zhan, L. Liu, H. Suo, Z.H. Ni, T.T. Nguyen, C. Zhao, and Z.X. Shen, *ACS nano* **5**, 147–152 (2011).
- (8) Y. You, T. Yu, J. Kasim, H. Song, X. Fan, Z. Ni, L. Cao, H. Jiang, D. Shen, J. Kuo, and Z. Shen, *Appl. Phys. Lett.* **93**, 103–111 (2008).
- (9) T. Yu, Z. Ni, C. Du, Y. You, Y. Wang, and Z. Shen, *J. Phys. Chem. C* **112**, 12602–12605 (2008).
- (10) C. Matthaus, A. Kale, T. Chernenko, V. Torchilin, and M. Diem, *Mol. Pharm.* **5**, 287–293 (2008).
- (11) T. Chernenko, C. Matthaus, L. Milane, L. Quintero, M. Amiji, and M. Diem, *ACS nano* **3**, 3552–3559 (2009).
- (12) <http://www.witec.de/en/download/Raman/StressinSi.pdf>.
- (13) T. Dieing, O. Hollricher, and J. Toporski, *Confocal Raman Microscopy*, (Springer, 2010) ISBN 978-3-642-12521-8.
- (14) C.A. Mack, *Microlithogr. World*, February edition, 14–15 (2004).
- (15) S. Wilhelm, B. Gröbler, M. Gluch, and H. Heinz, *Confocal Laser Scanning Microscopy*, <http://zeiss-campus.magnet.fsu.edu/referencelibrary/pdfs/Zeiss-ConfocalPrinciples.pdf>.

Thomas Dieing, PhD, Marius Henrich, and Sonja Breuninger, PhD, are with WITec GmbH in Ulm, Germany. Direct correspondence to: sonja.breuninger@witec.de ■

For more information on this topic, please visit our homepage at: www.spectroscopyonline.com

Confident Identification When it Matters Most



Push the Limits of Detection with Ocean Optics

Trace level detection of analytes ranging from adulterants to explosives is now simpler to accomplish with new Raman detection systems and measurement substrates. Combine our IDRaman benchtop or handheld systems with surface-enhanced Raman spectroscopy (SERS) substrates to maximize sensitivity. IDRaman's Raster Orbital Scanning (ROS) technique overcomes limitations of other sampling methods and takes full advantage of the enhanced signal intensity provided by the SERS substrates.



www.oceanoptics.com | info@oceanoptics.com

US +1 727-733-2447 EUROPE +31 26-3190500 ASIA +86 21-6295-6600

HORIBA

Scientific



The Art of RAMAN!

HORIBA Scientific offers a complete spectrum of Raman solutions that transforms Raman from a complicated science to an easy art form. From our new **XploRA™ Plus** fully confocal microscope, to our **LabRAM HR Evolution**, you will find an easy-to-use Raman instrument designed to fit your requirements and your budget, without needing to compromise. And, our instruments are backed by unsurpassed application and customer support, all from HORIBA Scientific, the leader in Raman spectroscopy.



www.horiba.com/raman
email: adsci-specty@horiba.com

HORIBA Scientific,
the Leader in
Raman Spectroscopy.

